Molecular Dynamics Study of Adsorption of the Lennard-Jones Truncated and Shifted Fluid on Planar Walls

Michaela Heier,[†] Felix Diewald,[‡] Martin T. Horsch,[†,¶] Kai Langenbach,[*,†] Ralf Müller,[‡] and Hans Hasse[†]

[†]*Laboratory of Engineering Thermodynamics, Technische Universität Kaiserslautern, Kaiserslautern, Germany*

[‡]*Institute of Applied Mechanics, Technische Universität Kaiserslautern, Kaiserslautern, Germany*

[¶]*Current address: Scientific Computing Division, STFC Daresbury Laboratory, UK Research and Innovation, Warrington, United Kingdom*

E-mail: kai.langenbach@mv-uni-kl.de

Phone: +49 (0)631 2054685. Fax: +49 (0)631 2053835

Abstract

A comprehensive molecular dynamics study of gas phase and supercritical fluid adsorption on planar walls in dispersive systems is presented. All interactions in the system are described with the Lennard-Jones truncated and shifted (LJTS) potential with a cut-off radius of 2.5 fluid diameters. The adsorption strength is characterized by the solid-fluid interaction energy and the wall density. Both parameters are varied systematically. The present work extends a previous study in which wetting in the same systems was investigated. Therefore the contact angles are known for all studied

systems. They include cases with total wetting as well as cases with partial wetting. The temperature varies between the triple point and three times the critical temperature of the LJTS fluid. For the systems with partial wetting, the adsorption is not only studied up to the saturation pressure, but also in the metastable region. For all systems, the surface excess is determined as a function of pressure and temperature. Furthermore, data on the thickness and structure of the adsorption are reported. In some of the systems, prewetting is observed.

Introduction

Adsorption and wetting are related phenomena. In a recent study, we have systematically investigated the wetting in dispersive systems by molecular dynamics (MD) simulations.[1] This study is extended here to adsorption. The fluid phase is gaseous or supercritical, the surface is flat. As in the previous study, all interactions are described by the Lennard-Jones truncated and shifted (LJTS) potential with a cut-off radius of 2.5 fluid diameters.

The LJTS model is probably the simplest molecular model with which properties of fluids can be described quantitatively for a wide range of states. It has therefore been used extensively as a model fluid[1–8,8–15] and its properties are well known.[1,2,8–10,16–20]

There are several previous studies in the literature that report on adsorption in dispersive systems with planar walls.[21–30] They were carried out either with molecular simulations or with density functional theory (DFT). In related studies of dispersive systems, the adsorption in slit pores or cylindrical pores was investigated.[29–40] In all available DFT studies, but also in many molecular simulation studies, the wall is described by a surface potential that is a scalar function of the distance to the flat surface, namely by LJ-9-3[21,23–25,27–29,31–34] and the LJ-10-4-3[29,30,34–39,41] potentials. In the present work, we study the adsorption on atomistic walls.

Adsorption isotherms in dispersive systems show different patterns. For contact angles greater than 0° (partial wetting) thin-film adsorption is observed and the surface excess

increases with increasing pressure until the saturation pressure is reached. The surface excess remains finite at the saturation pressure.[23,42] For systems with a contact angle of $\theta = 0°$ (total wetting) the surface excess diverges at the saturation pressure (thick-film adsorption). For systems with small contact angles, i.e. near the transition between partial and total wetting prewetting is observed at pressures near the saturation pressure.[42,43] At saturation pressure, the surface excess diverges. Prewetting is a discontinuous transition between thin-film and thick film adsorption.[23] This wetting transition was first predicted by Cahn[44] and Ebner and Saam[45] independently. Pandit et al.[46] associated the wetting regimes with the different shapes of adsorption isotherms and Finn and Monson[23] proved the existence of the prewetting by Monte Carlo simulations for the first time.

To the best of the authors' knowledge, gas phase adsorption isotherms have so far only been studied up to the saturation pressure. It is known that metastable states in gas phases can be studied by molecular dynamics simulations.[5] In the present study, adsorption isotherms are also reported for pressures above the saturation pressure, i.e. for conditions for which the gas phase is metastable. The pressure was increased until droplet formation was observed. Becker et al.[1] have shown that contact angles determined in dispersive systems modeled with LJTS potential with $r_c = 2.5\ \sigma$ agree well with literature data obtained with other variants of the Lennard-Jones potential and that also the differences between site-based wall models and planar wall potentials of the LJ type were small as long as the energy parameters were chosen consistently.

The present work reports on a comprehensive study of gas phase and supercritical fluid adsorption in LJTS systems. The adsorption strength is systematically varied by varying the solid-fluid interaction energy as well as the wall density. The contact angles are known for all studied systems from our previous investigation.[1] Cases with total wetting as well as cases with partial wetting are considered. The temperature is varied in a wide range between the triple point and three times the critical temperature of the LJTS fluid. All in all, 49 adsorption isotherms with 4 to 14 data points per isotherm are reported together

with information on the thickness and structure of the adsorption layer and the contact angle.

Molecular Simulation

Molecular Model

To describe the interaction between particles, the LJTS-12-6 potential u_{LJTS} is used, which is based on the LJ-12-6 potential u_{LJ}:

$$u_{\mathrm{LJ}}(r) = 4\varepsilon \left[\left(\frac{\sigma}{r}\right)^{12} - \left(\frac{\sigma}{r}\right)^{6} \right] \tag{1}$$

$$u_{\mathrm{LJTS}}(r) = \begin{cases} u_{\mathrm{LJ}}(r) - u_{\mathrm{LJ}}(r_{\mathrm{c}}) & r \leq r_{\mathrm{c}} \\ 0 & r > r_{\mathrm{c}} \end{cases} . \tag{2}$$

ε and σ are the energy and size parameter respectively and r is the distance between two particles.[47] The LJTS potential is truncated and shifted at a cut-off radius, which is $r_{\mathrm{c}} = 2.5\,\sigma$ throughout the present work. All properties are normalized using ε and σ of the fluid (f). The energy parameter of the solid (s) is $\varepsilon_{\mathrm{s}} = 100\ \varepsilon_{\mathrm{f}}$, whereas the energy parameter of the solid-fluid (sf) interaction is calculated using:

$$\varepsilon_{\mathrm{sf}} = \zeta\ \varepsilon_{\mathrm{f}}, \tag{3}$$

where ζ is the reduced solid-fluid interaction energy which is varied from 0.35 to 2.0. The LJTS sites of the solid are not fixed, i.e. they fully take part in the simulation. However, due to the strong attraction, they remain in the crystal configuration which is specified at the start of the simulation. Here, this is a face-centered cubic (fcc) lattice with the (100) surface exposed to the fluid. The density of the solid is changed by varying the size of the LJTS sites of the solid σ_{s}. The lattice constant of the solid is $a = 1.55\ \sigma_{\mathrm{s}}$. Table 1 shows

the size parameters and densities of the solids used in this work.

The influence of the solid-fluid interaction and the solid density on the adsorption is described using the average minimum potential W. It was already used successfully by Becker et al.[1] to describe the contact angle as a function of the solid-fluid interaction, solid density, and the temperature. W is defined as:

$$W = -\frac{1}{L_x L_z} \int_0^{L_z} \int_0^{L_x} u_{\min}^{\sum}(x, z) \, \mathrm{d}x \, \mathrm{d}z. \tag{4}$$

Here, x and z are Cartesian coordinates in the surface plane and L_x and L_z the corresponding dimensions of the rectangular plane. The term $u_{\min}^{\sum}(x, z)$ is the cumulative minimum potential at a given lateral position (x, z). The cumulative potential $u^{\sum}(x, y, z)$ describes the interaction of one fluid particle with all wall particles.[48] It depends on the density of the wall, the distance y between the fluid particle and the wall, and the position of the fluid particle in lateral (x, z) position. For any position (x, z) on the wall, it has a minimum $u_{\min}^{\sum}(x, z)$ at some distance y^* above the wall. W depends linearly on ζ for the LJTS potential and on the solid density ρ_s. Becker et al.[1] used the method of Grzelak et al.[49] to calculate W for the solids used in this work. The results for W are shown in Table 1.

Simulation Method

Molecular dynamics (MD) simulations were carried out with the massively parallel code *ls1 mardyn*[15] in a canonical (NVT) ensemble. A scheme of the simulation scenario is depicted in Figure 1.

[Figure 1 near here]

The scenario contains an atomistic wall which is fixed at the bottom of the simulation box as described in the Supplementary Information. The surface of the wall is located in

the x,z-plane, the y coordinate is perpendicular to that plane. The wall has 6 layers of sites such that its thickness is larger than $r_c = 2.5\ \sigma_f$ and no periodic artifacts occur. In x-, y-, and z-direction periodic boundary conditions are applied. Near the top of the simulation box at a height of $y = 55\ \sigma_f$ a repulsive soft membrane is applied. This membrane avoids the layer growth underneath the atomistic wall, which would appear due to periodic boundary conditions in y-direction. For details, see the Supplementary Information. The distance from the surface of the solid wall to the membrane is bigger than 40 σ_f such that the influence of the membrane on the adsorption process is negligible.[29]

The width and the depth of the simulation box are the same ($\Delta x = \Delta z$). The numbers for Δx, Δz, and N_f are determined from the fluid density. N_f is at least 8,000 and Δx and Δz are at least 50 σ_f. Results from a preliminary study on the influence of the choice of N_f on the results for the adsorption showed that no size effects are present for N_f larger than 6,000, see the Supplementary Information. The studied temperature range covers subcritical and supercritical temperatures from the triple point to three times the temperature at the critical point ($T_{TP} = 0.65\ \varepsilon_f k^{-1}$, $T_c = 1.0779\ \varepsilon_f k^{-1}$).[2,18] The temperature is kept constant by an Andersen thermostat[50] with a collision frequency of $\nu = 0.05$. In the initial configuration, the fluid particles are equally distributed. During the simulation fluid particles are attracted by the wall and form an adsorption layer. The equilibration time of a simulation is at least 1 million time steps with a simulation time step of $\Delta t = 0.0005\ (m/\varepsilon_f)^{1/2}\sigma_f$. The equilibration is followed by a production run of 2.5 million time steps.

Table 2 gives an overview of all adsorption isotherms that were studied in the present work. For each adsorption isotherm 4 - 14 simulations for different pressures were carried out while all other conditions were kept constant. The pressure is set indirectly by the number of fluid particles in the simulation volume.

[Table 2 near here]

Data evaluation

Fluid density profiles $\rho_{\mathrm{f}}(y)$ and pressure profiles $p_{\mathrm{f}}(y)$ were sampled during the simulation runs using 400 bins of equal size in y-direction. Density was sampled by counting the particles per bin and pressure, defined as one third of the trace of the pressure tensor, was sampled using the intermolecular virial.[51] Block averages were determined for each bin with a block size of 500,000 time steps. Figure 2 shows examples of a fluid density profile $\rho_{\mathrm{f}}(y)$ and pressure profile $p_{\mathrm{f}}(y)$.

[Figure 2 near here]

For $y < y_{\mathrm{n}}$ the fluid density and the fluid pressure are zero, because this region belongs to the wall. On the other hand, if y exceeds a certain threshold ($y > y_{\mathrm{b}}$) the fluid density $\rho_{\mathrm{f}}(y)$ and the fluid pressure $p_{\mathrm{f}}(y)$ are constant and equal to the bulk fluid density $\rho_{\mathrm{f}}^{\mathrm{b}}$ and bulk fluid pressure $p_{\mathrm{f}}^{\mathrm{b}}$. Only at high values of y, the influence of the membrane is observed ($y > y_1 = 55\,\sigma_{\mathrm{f}}$). For $y_0 < y < y_{\mathrm{b}}$ the adsorption results in a layering structure in the density profile. In the case shown in Figure 2, two density peaks are observed in this interval. Also the pressure profile shows oscillations which result from the layering. The bulk fluid density $\rho_{\mathrm{f}}^{\mathrm{b}}$ and the bulk fluid pressure $p_{\mathrm{f}}^{\mathrm{b}}$ are calculated by averaging the respective values between y_{b} and y_1, cf. Figure 2. Numbers for y_{b} are needed here only for determining these bulk values. y_{b} was chosen in such a way that for $y > y_{\mathrm{b}}$ the profiles were constant within the scattering of the data.

The surface excess Γ is calculated from $\rho_{\mathrm{f}}(y)$ using Equation 5:[52]

$$\Gamma = \int_{y_0}^{y_1} \left[\rho_{\mathrm{f}}(y) - \rho_{\mathrm{f}}^{\mathrm{b}}\right] \, \mathrm{d}y. \tag{5}$$

The integration starts at y_0, which is the first intersection of the density profile with the bulk density and the integration ends at y_1. Both integration values are depicted in Figure 2.

The layer thickness is calculated here from:

$$\delta = y_{\mathrm{u}} - y_{\mathrm{l}}. \tag{6}$$

The lower bound of $y = y_{\mathrm{l}}$ is determined by the first rise in the density profile $\rho_{\mathrm{f}}(y)$ and is not difficult to assign. The position y_{l} is always near $y_{\mathrm{max}}-0.5\ \sigma_{\mathrm{f}}$ where y_{max} is the position of the first maximum of the density. For simplicity, therefore, $y_{\mathrm{l}} = y_{\mathrm{max}} - 0.5\ \sigma_{\mathrm{f}}$ is used here throughout. There is more arbitrariness in determining the upper bound y_{u}. Using y_{b} would not be a good choice as its number depends on the scattering of the data and very large. As a result scattering numbers for δ would be obtained. Here, y_{u} is simply found from the intersection of the density profile with 1.1 $\rho_{\mathrm{f}}^{\mathrm{b}}$. δ is also shown in Figure 2. The density profiles $\rho_{\mathrm{f}}(y)$ and the pressure profiles $p_{\mathrm{f}}(y)$ are uniquely determined by the wall properties, number of particles, volume, and temperature of a given simulation run. In Figure 3 examples for density profiles with 1, 2, 3, and 4 peaks are shown.

[Figure 3 near here]

The uncertainty of the simulation data that is reported here is three times the standard deviation of the production run. The data for averaged (over 2,500,000 time steps) fluid density profiles $\rho_{\mathrm{f}}^{*}(y)$ and the uncertainty $\Delta\rho_{\mathrm{f}}^{*}(y)$ is given for all simulations in the Excel sheet in the Supplementary Information.

Results and Discussion

In this paragraph, first results for one subcritical and one supercritical temperature are discussed in detail. Then the rest of the results is presented. Numerical results for $\rho_\mathrm{f}^\mathrm{b}$, p_f^b, Γ, δ, and number of adsorption peaks N_peaks are reported in the Supplementary Information.

Adsorption Isotherms for $T/T_\mathrm{c} = 0.8$

Figure 4 shows the surface excess Γ as a function of the bulk fluid pressure p_f^b for $T/T_\mathrm{c} = 0.8$ for different values of the reduced solid-fluid interaction energy ζ and the solid density ρ_s.

[Figure 4 near here]

A contact angle is assigned to each adsorption isotherm based on the work of Becker et al.[1] The contact angles for $\rho_\mathrm{s} = 1.07\ \sigma_\mathrm{f}^{-3}$ are calculated using Equation (9) of Becker et al.[1] The others are described by Heier et al.[53] Figure 4 also contains information on the saturation pressure p_f^s which is calculated using a correlation of Vrabec et al.[2] and is shown as a dashed line. For increasing pressure, the adsorption isotherms with $\theta = 0°$ go to infinity at the saturation pressure for all solid densities. For $\theta = 11.2°$ ($W = 2.31$, top) a wetting transition from partial to total wetting is observed, which is indicated by a jump in the adsorption isotherm at $p_\mathrm{f}^\mathrm{b} = 0.022\ \varepsilon\sigma_\mathrm{f}^{-3}$. This jump appears between the filled symbols in the top diagram of Figure 4. At the saturation pressure this isotherm also goes to infinity as well. For larger values of θ the adsorption isotherms remain finite at the saturation pressure. In that regime, also simulations for pressures above the saturation pressure, i.e. in the metastable region of the fluid, were performed. The pressure was increased until droplet formation occurred. Further information on the droplet formation can be found in the Supplementary Information. In the simulations with metastable conditions for which adsorption data are reported here, no nucleation events were observed. Horsch et al.[4,54] investigated

nucleation for the supersaturated LJTS fluid with $r_c = 2.5\ \sigma_f$ with molecular simulations and classical nucleation theory. The fact that no nucleation was observed in the simulations with metastable fluids for which data are reported here is in accordance with the results of that work. For the system size and number of particles in the simulations of the present work no nucleation events are expected if the pressure is not increased further. To summarize, the surface excess at fixed temperatures increases for: increasing W, solid density, and reduced solid-fluid interaction energy. For the contact angle $\theta = 11.2°$ a wetting transition occurs. For small contact angles the surface excess diverges at the saturation pressure while for large contact angles it remains finite even in the metastable range.

Figure 5 shows the adsorption layer thickness δ as a function of p_f^b for $T/T_c = 0.8$ for different values of the reduced solid-fluid interaction energy ζ and the solid density ρ_s.

[Figure 5 near here.]

The curves $\delta(p_f^b)$ are called δ-curves in the following. They are similar to the corresponding adsorption isotherms. For $\theta = 11.2°$ a jump can also be seen in the δ-curve were the wetting transition occurs. Contrary to what might be expected for a monolayer, δ does not converge to σ_f for low pressures, but to values that are higher. This is due to the slow decay of the density profile on the vapor side, compare Figure 2, that results in the fact that even for monolayers δ, as defined by Equation 6, is larger than σ_f. The second, third, and fourth layer occur for larger values of δ. The number of peaks for each simulation point is indicated by different symbols in Figure 5.

Adsorption for $T/T_c = 1.1$

Figure 6 shows the surface excess Γ as a function of the bulk fluid pressure p_f^b for $T/T_c = 1.1$ for different values of the reduced solid-fluid interaction energy ζ and the solid density ρ_s.

[Figure 6 near here]

A comparison of Figures 5 and 6 shows that the shapes of the adsorption isotherms for $T/T_c = 1.1$ differ significantly from those for $T/T_c = 0.8$. For $T < T_c$ the adsorption isotherms have a convex shape or an s-shape, for $T > T_c$ the adsorption isotherms are concave and converge to a constant surface excess. However, the following observations are similar to the observations made for $T < T_c$: First, the surface excess increases with increasing W for constant temperature and solid density. Second, the surface excess increases for increasing solid density and increasing reduced solid-fluid interaction energy. Except for the shape of the adsorption isotherms the basic behavior of the adsorption isotherms (with regard to ζ and ρ_s) is the same for subcritical or supercritical adsorption. At constant other conditions, the surface excess decreases with increasing temperature.
The δ-curves for $T/T_c = 1.1$ are shown in Figure 7.

[Figure 7 near here.]

The δ-curves are again similar to the adsorption isotherms. The layer thickness decreases with increasing temperature.

Adsorption for $T/T_c = 0.7$, 0.77, 0.9, 1.5, 2.0, and 3.0

Adsorption isotherms for $T/T_c = 0.7$, 0.77, 0.9, 1.5, 2.0, and 3.0 are shown in Figure 8, 9, 10, 11, 12, and 13 respectively.

[Figure 8 near here]

[Figure 9 near here]

[Figure 10 near here]

[Figure 11 near here]

[Figure 12 near here]

[Figure 13 near here]

In these Figures it can be seen that the behavior of the subcritical adsorption isotherms is similar to that for $T/T_c = 0.8$ discussed above. The supercritical isotherms resemble that for $T/T_c = 1.1$.

For $T/T_c = 0.9$ no simulation results in the metastable region were obtained as nucleation was observed in all attempts. Droplet growth at the wall as well as important clustering of particles in the vapor phase were even observed for pressures slightly below the saturation pressure. For high temperatures (i.e. $T/T_c = 1.5$, 2.0, and 3.0) the surface excess is so small that the calculation of the adsorption layer thickness becomes difficult. Therefore no data on δ is reported for these cases. The results for δ for the other cases are shown in the Supplementary Information.

The bulk fluid values ρ_f^b and p_f^b from the adsorption simulations in the stable and metastable range are compared to PeTS EOS[5] predictions in Figure 14. PeTS EOS is known to be accurate in the metastable range. The agreement is very good. This confirms the accuracy of the present metastable simulations.

[Figure 14 near here]

Conclusion

Gas and supercritical adsorption on a planar wall in dispersive systems was investigated in the present work by molecular dynamics simulations. The Lennard-Jones truncated and shifted (LJTS) potential with a cut-off radius of 2.5 fluid diameters was used for describing the fluid-fluid, solid-fluid, and solid-solid interactions. Adsorption simulations were performed for $T/T_c = 0.7$, 0.77, 0.8, 0.9, 1.1, 1.5, 2.0, and 3.0 for a wide range of solid-fluid interaction and solid density which determine the strength of the adsorption. The molecular parameters that determine the adsorption strength also determine the contact angle. From a previous work on wetting in the same systems, the contact angles are known for all adsorption isotherms studied here. To the authors knowledge, adsorption was studied here for the first time in the metastable region. For small contact angles, prewetting is observed in a narrow range. In general, for decreasing temperature, increasing solid density, and increasing reduced solid-fluid interaction energy the surface excess increases.

This work gives a comprehensive dataset for describing the adsorption in dispersive systems for a wide range of conditions which could be used e.g. for evaluating density functional theory and density gradient theory.

Acknowledgement

The authors gratefully acknowledge funding of the present work by Deutsche Forschungsgemeinschaft DFG within CRC 926. They acknowledge computational support by the Leibniz Supercomputing Center (LRZ) under the large-scale grant SPARLAMPE (pr48te) and the Regional University Computing Center Kaiserslautern (RHRK) under the grant TUK-TLMV. The present work was conducted under the auspices of the Boltzmann-Zuse Society for Computational Molecular Engineering (BZS).

Supporting Information Available

The following files are available free of charge.

- Supplementary Information: The Supplementary Information contains further information regarding the simulation scenario, the size effect, the adsorption results, and the detection of a droplet growth in the metastable region. A table with all results of the adsorption simulations is shown.
- An additional Excel-Sheet is provided with averaged density profiles $\rho_{\mathrm{f}}^{*}(y)$ for all adsorption simulations.

References

(1) Becker, S.; Urbassek, H. M.; Horsch, M.; Hasse, H. Contact Angle of Sessile Drops in Lennard-Jones Systems. *Langmuir* **2014**, *30*, 13606–13614.

(2) Vrabec, J.; Kedia, G. K.; Fuchs, G.; Hasse, H. Comprehensive study of the vapour-liquid coexistence of the truncated and shifted Lennard-Jones fluid including planar and spherical interface properties. *Molecular Physics* **2006**, *104*, 1509–1527.

(3) Becker, S.; Kohns, M.; Urbassek, H. M.; Horsch, M.; Hasse, H. Static and Dynamic Wetting Behavior of Drops on Impregnated Structured Walls by Molecular Dynamics Simulation. *The Journal of Physical Chemistry C* **2017**, *121*, 12669–12683.

(4) Horsch, M.; Vrabec, J.; Hasse, H. Modification of the classical nucleation theory based on molecular simulation data for surface tension, critical nucleus size, and nucleation rate. *Physical Review E* **2008**, *78*, 011603.

(5) Heier, M.; Stephan, S.; Liu, J.; Chapman, W. G.; Hasse, H.; Langenbach, K. Equation of state for the Lennard-Jones truncated and shifted fluid with a cut-off radius of 2.5 σ based on perturbation theory and its applications to interfacial thermodynamics. *Molecular Physics* **2018**, *116*, 2083–2094.

(6) Horsch, M.; Hasse, H. Molecular simulation of nano-dispersed fluid phases. *Chemical Engineering Science* **2014**, *107*, 235–244.

(7) Lautenschlaeger, M. P.; Stephan, S.; Horsch, M. T.; Kirsch, B.; Aurich, J. C.; Hasse, H. Effects of Lubrication on Friction and Heat Transfer in Machining Processes on the Nanoscale: A Molecular Dynamics Approach. *Procedia CIRP* **2018**, *67*, 296–301.

(8) Horsch, M.; Heitzig, M.; Dan, C.; Harting, J.; Hasse, H.; Vrabec, J. Contact Angle Dependence on the Fluid-Wall Dispersive Energy. *Langmuir* **2010**, *26*, 10913–10917.

(9) Horsch, M.; Hasse, H.; Shchekin, A. K.; Agarwal, A.; Eckelsbach, S.; Vrabec, J.; Müller, E. A.; Jackson, G. Excess equimolar radius of liquid drops. *Physical Review E* **2012**, *85*, 031605.

(10) Lotfi, A.; Vrabec, J.; Fischer, J. Evaporation from a free liquid surface. *International Journal of Heat and Mass Transfer* **2014**, *73*, 303–317.

(11) Heinen, M.; Vrabec, J.; Fischer, J. Communication: Evaporation: Influence of heat transport in the liquid on the interface temperature and the particle flux. *The Journal of Chemical Physics* **2016**, *145*, 081101.

(12) Horsch, M.; Miroshnichenko, S.; Vrabec, J. Steady-state molecular dynamics simulation of vapour to liquid nucleation with McDonald's daemon. *Journal of Physical Studies* **2009**, *13*, 4004.

(13) Eckhardt, W.; Heinecke, A.; Bader, R.; Brehm, M.; Hammer, N.; Huber, H.; Kleinhenz, H.-G.; Vrabec, J.; Hasse, H.; Horsch, M.; Bernreuther, M.; Glass, C. W.; Niethammer, C.; Bode, A.; Bungartz, H.-J. 591 TFLOPS Multi-trillion Particles Simulation on SuperMUC. Supercomputing. Berlin, Heidelberg, 2013; pp 1–12.

(14) Werth, S.; Lishchuk, S. V.; Horsch, M.; Hasse, H. The influence of the liquid slab thickness on the planar vapor-liquid interfacial tension. *Physica A: Statistical Mechanics and its Applications* **2013**, *392*, 2359–2367.

(15) Niethammer, C.; Becker, S.; Bernreuther, M.; Buchholz, M.; Eckhardt, W.; Heinecke, A.; Werth, S.; Bungartz, H.-J.; Glass, C. W.; Hasse, H.; Vrabec, J.; Horsch, M. ls1 mardyn: The Massively Parallel Molecular Dynamics Code for Large Systems. *Journal of Chemical Theory and Computation* **2014**, *10*, 4455–4464.

(16) Smit, B.; Frenkel, D. Vapor-liquid equilibria of the two-dimensional Lennard-Jones fluid(s). *The Journal of Chemical Physics* **1991**, *94*, 5663–5668.

(17) Smit, B. Phase diagrams of Lennard-Jones fluids. *The Journal of Chemical Physics* **1992**, *96*, 8639–8640.

(18) van Meel, J. A.; Page, A. J.; Sear, R. P.; Frenkel, D. Two-step vapor-crystal nucleation close below triple point. *The Journal of Chemical Physics* **2008**, *129*, 204505.

(19) Rusanov, A. I.; Brodskaya, E. N. The molecular dynamics simulation of a small drop. *Journal of Colloid and Interface Science* **1977**, *62*, 542–555.

(20) Landry, E. S.; Mikkilineni, S.; Paharia, M.; McGaughey, A. J. H. Droplet evaporation: A molecular dynamics investigation. *Journal of Applied Physics* **2007**, *102*, 124301.

(21) Sweatman, M. B. Weighted density-functional theory for simple fluids: Prewetting of a Lennard-Jones fluid. *Physical Review E* **2001**, *65*, 011102.

(22) Abraham, F. F. The interfacial density profile of a Lennard-Jones fluid in contact with a (100) Lennard-Jones wall and its relationship to idealized fluid/wall systems: A Monte Carlo simulation. *The Journal of Chemical Physics* **1978**, *68*, 3713–3716.

(23) Finn, J. E.; Monson, P. A. Prewetting at a fluid-solid interface via Monte Carlo simulation. *Physical Review A* **1989**, *39*, 6402–6408.

(24) Fan, Y.; Monson, P. A. Further studies of prewetting transitions via Monte Carlo simulation. *The Journal of Chemical Physics* **1993**, *99*, 6897–6906.

(25) Yang-Xin, Y.; Ying-Feng, L.; Yuan-Xiang, Z. Thin-Thick Film Transitions on a Planar Solid Surface: A Density Functional Study. *Chinese Physics Letters* **2010**, *27*, 037101.

(26) Saville, G. Computer simulation of the liquid-solid-vapour contact angle. *Journal of the Chemical Society, Faraday Transactions 2: Molecular and Chemical Physics* **1977**, *73*, 1122–1132.

(27) Errington, J. R. Prewetting Transitions for a Model Argon on Solid Carbon Dioxide System. *Langmuir* **2004**, *20*, 3798–3804.

(28) Toxvaerd, S. Molecular Dynamics Simulation of Prewetting. *The Journal of Physical Chemistry C* **2007**, *111*, 15620–15624.

(29) Oleinikova, A.; Brovchenko, I.; Geiger, A. Behavior of a wetting phase near a solid boundary: vapor near a weakly attractive surface. *The European Physical Journal B - Condensed Matter and Complex Systems* **2006**, *52*, 507–519.

(30) Yu, Y.-X. A novel weighted density functional theory for adsorption, fluid-solid interfacial tension, and disjoining properties of simple liquid films on planar solid surfaces. *The Journal of Chemical Physics* **2009**, *131*, 024704.

(31) Peterson, B. K.; Gubbins, K. E.; Heffelfinger, G. S.; Marini Bettolo Marconi, U.; van Swol, F. Lennard-Jones fluids in cylindrical pores: Nonlocal theory and computer simulation. *The Journal of Chemical Physics* **1988**, *88*, 6487–6500.

(32) Tan, Z.; Swol, F. V.; Gubbins, K. E. Lennard-Jones mixtures in cylindrical pores. *Molecular Physics* **1987**, *62*, 1213–1224.

(33) Sokolowski, S.; Fischer, J. Lennard-Jones mixtures in slit-like pores: a comparison of simulation and density-functional theory. *Molecular Physics* **1990**, *71*, 393–412.

(34) Choudhury, N.; Ghosh, S. K. Adsorption of Lennard-Jones fluid mixture in a planar slit: A perturbative density functional approach. *Physical Review E* **2001**, *64*, 021206.

(35) Cracknell, R. F.; Nicholson, D.; Quirke, N. A grand canonical Monte Carlo study of Lennard-Jones mixtures in slit shaped pores. *Molecular Physics* **1993**, *80*, 885–897.

(36) Sweatman, M. B. Weighted density functional theory for simple fluids: Supercritical adsorption of a Lennard-Jones fluid in an ideal slit pore. *Physical Review E* **2001**, *63*, 031102.

(37) Ravikovitch, P. I.; Vishnyakov, A.; Neimark, A. V. Density functional theories and

molecular simulations of adsorption and phase transitions in nanopores. *Physical Review E* **2001**, *64*, 011602.

(38) Walton, J. P. R. B.; Quirke, N. Capillary Condensation: A Molecular Simulation Study. *Molecular Simulation* **1989**, *2*, 361–391.

(39) Peng, B.; Yu, Y.-X. A Density Functional Theory with a Mean-field Weight Function: Applications to Surface Tension, Adsorption, and Phase Transition of a Lennard-Jones Fluid in a Slit-like Pore. *The Journal of Physical Chemistry B* **2008**, *112*, 15407–15416.

(40) Panagiotopoulos, A. Z. Adsorption and capillary condensation of fluids in cylindrical pores by Monte Carlo simulation in the Gibbs ensemble. *Molecular Physics* **1987**, *62*, 701–719.

(41) Maddox, M. W.; Gubbins, K. E. A molecular simulation study of freezing/melting phenomena for Lennard-Jones methane in cylindrical nanoscale pores. *The Journal of Chemical Physics* **1997**, *107*, 9659–9667.

(42) Dietrich, S. In *Phase Transitions and Critical Phenomena*; Domb, S., Lebowitz, J., Eds.; Academic Press: London, 1988; Vol. 12.

(43) Bonn, D.; Ross, D. Wetting transitions. *Reports on Progress in Physics* **2001**, *64*, 1085.

(44) Cahn, J. W. Critical point wetting. *The Journal of Chemical Physics* **1977**, *66*, 3667–3672.

(45) Ebner, C.; Saam, W. F. New Phase-Transition Phenomena in Thin Argon Films. *Physical Review Letters* **1977**, *38*, 1486–1489.

(46) Pandit, R.; Schick, M.; Wortis, M. Systematics of multilayer adsorption phenomena on attractive substrates. *Physical Review B* **1982**, *26*, 5112–5140.

(47) Allen, M. P.; Tildesley, D. J. *Computer simulation of liquids*; Oxford university press: Oxford, 1989.

(48) Hamaker, H. C. The London-van der Waals attraction between spherical particles. *Physica* **1937**, *4*, 1058–1072.

(49) Grzelak, E. M.; Shen, V. K.; Errington, J. R. Molecular Simulation Study of Anisotropic Wetting. *Langmuir* **2010**, *26*, 8274–8281.

(50) Andersen, H. C. Molecular dynamics simulations at constant pressure and/or temperature. *The Journal of Chemical Physics* **1980**, *72*, 2384–2393.

(51) Walton, J. P. R. B.; Tildesley, D. J.; Rowlinson, J. S.; Henderson, J. R. The pressure tensor at the planar surface of a liquid. *Molecular Physics* **1983**, *48*, 1357–1368.

(52) Findenegg, G. H.; Fischer, J. Adsorption of fluids: simple theories for the density profile in a fluid near an adsorbing surface. *Faraday Discussions of the Chemical Society* **1975**, *59*, 38–45.

(53) Heier, M.; Becker, S.; Urbassek, H. M.; Horsch, M.; Hasse, H. Correction to "Contact Angle of Sessile Drops in Lennard-Jones Systems". *Langmuir* **2018**, *34*, 3374–3374.

(54) Horsch, M.; Vrabec, J. Grand canonical steady-state simulation of nucleation. *The Journal of Chemical Physics* **2009**, *131*, 184104.

Tables

Table 1: Size parameter σ_s, density ρ_s, and average minimum potential W of the studied LJTS solid walls.

σ_s/σ_f	0.646	0.8	1
ρ_s/σ_f^{-3}	3.98	2.10	1.07
$W/\zeta kT_c$	8.07	4.83	3.08

Table 2: Overview of the conditions for which the adsorption was studied in the present work.

T/T_c	ρ_s/σ_f^{-3}	ζ	$W/(kT_c)$	$\theta/^\circ$
0.7	1.07	0.35	1.08	123.82
		0.514	1.58	90
		0.65	2.00	62.51
		0.75	2.31	36.78
0.77	1.07	0.75	2.31	24.05
0.8	1.07	0.35	1.08	132.98
		0.514	1.58	90
		0.65	2.00	55.57
		0.75	2.31	11.17
		1.0	3.08	0
		1.5	4.62	0
		2.0	6.16	0
	2.1	0.35	1.69	101.40
		0.514	2.48	41.53
		0.65	3.14	0
	3.98	0.35	2.83	74.93
		0.514	4.15	0
		0.65	5.25	0
0.9	1.07	0.35	1.08	175.04
		0.514	1.58	90
		0.65	2.00	34.39
		0.75	2.31	0
1.1	1.07	0.35	1.08	
		0.514	1.58	
		0.65	2.00	
		1.0	3.08	
		1.5	4.62	
		2.0	6.16	
	2.1	0.35	1.69	
		0.514	2.48	
		0.65	3.14	
	3.98	0.35	2.83	
		0.514	4.15	
		0.65	5.25	
1.5	1.07	0.35	1.08	
		0.514	1.58	

T/T_c	ρ_s/σ_f^{-3}	ζ	$W/(kT_c)$	$\theta/^\circ$
		0.65	2.00	
2.0	1.07	0.35	1.08	
		0.514	1.58	
		0.65	2.00	
3.0	1.07	0.35	1.08	
		0.514	1.58	
		0.65	2.00	
	2.1	0.35	1.69	
		0.514	2.48	
		0.65	3.14	
	3.98	0.35	2.83	
		0.514	4.15	
		0.65	5.25	
		0.514	2.48	
		0.65	3.14	

Figures

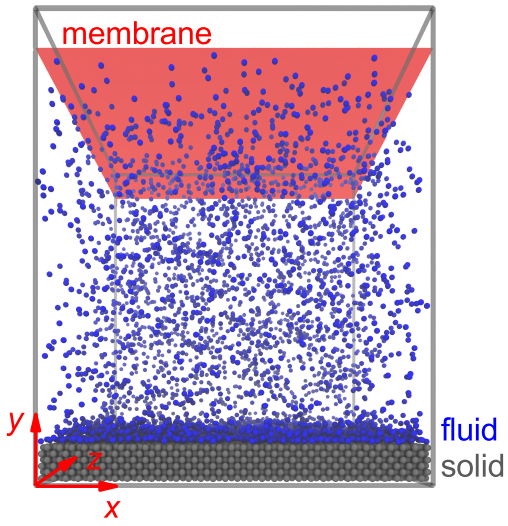

Figure 1: Snapshot of the adsorption simulation scenario. Periodic boundary conditions are applied in all directions. The solid wall on the top of the box is shielded by the membrane and is not depicted. [This Figure is 1 column wide]

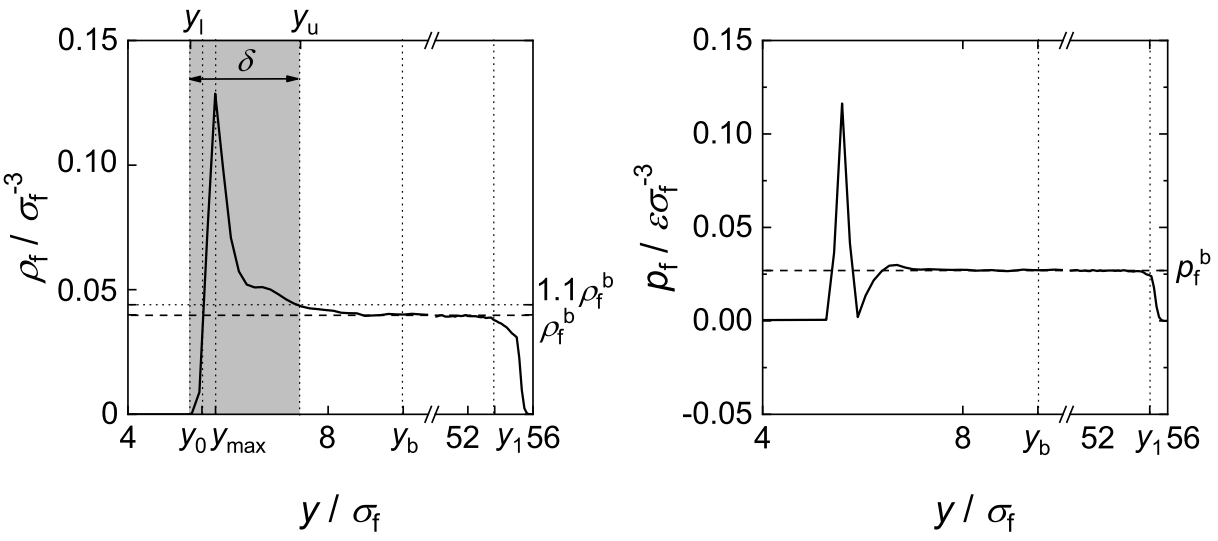

Figure 2: *Left:* Density profile of the fluid phase $\rho_\mathrm{f}(y)$ (solid line) for $T/T_\mathrm{c} = 0.8$, $\rho_\mathrm{s} = 1.07\ \sigma_\mathrm{f}^{-3}$, $\zeta = 0.65$, and $\rho_\mathrm{f}^\mathrm{b} = 0.0399\ \sigma_\mathrm{f}^{-3}$. The dashed line shows the bulk density $\rho_\mathrm{f}^\mathrm{b}$ of the vapor phase. y_0 and y_1 show the integration boundaries for the surface excess calculation, y_b is the start value for the bulk density calculation and y_max shows the y-coordinate of the first peak. y_l and y_u determine the layer thickness δ, which is shown by the gray area. $1.1\ \rho_\mathrm{f}^\mathrm{b}$ is used to calculated y_m and also shown. *Right:* Pressure profile of the fluid phase $p_\mathrm{f}(y)$ (solid line) for the same conditions. The dashed line shows the bulk pressure $p_\mathrm{f}^\mathrm{b}(y) = 0.0269\ \varepsilon\sigma_\mathrm{f}^{-3}$ of the vapor phase. y_b and y_1 show the start and end values of the bulk pressure calculation. [This Figure is 2 columns wide]

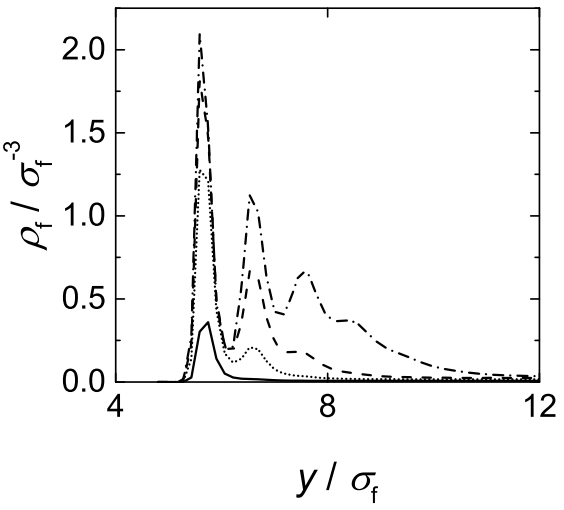

Figure 3: Density profiles of the fluid phase $\rho_{\mathrm{f}}(y)$ from four data points at different pressures from the isotherm $T/T_{\mathrm{c}} = 0.8$ for $\rho_{\mathrm{s}} = 1.07\ \sigma_{\mathrm{f}}^{-3}$ and $\zeta = 1.0$. Solid: $p_{\mathrm{f}}^{\mathrm{b}} = 0.00584$, dotted: $p_{\mathrm{f}}^{\mathrm{b}} = 0.01263$, dashed: $p_{\mathrm{f}}^{\mathrm{b}} = 0.0178$, dash-dotted: $p_{\mathrm{f}}^{\mathrm{b}} = 0.0223$. [This Figure is 1 column wide]

Graphical TOC Entry

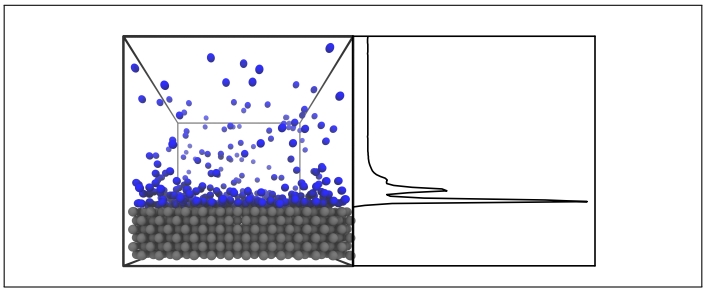

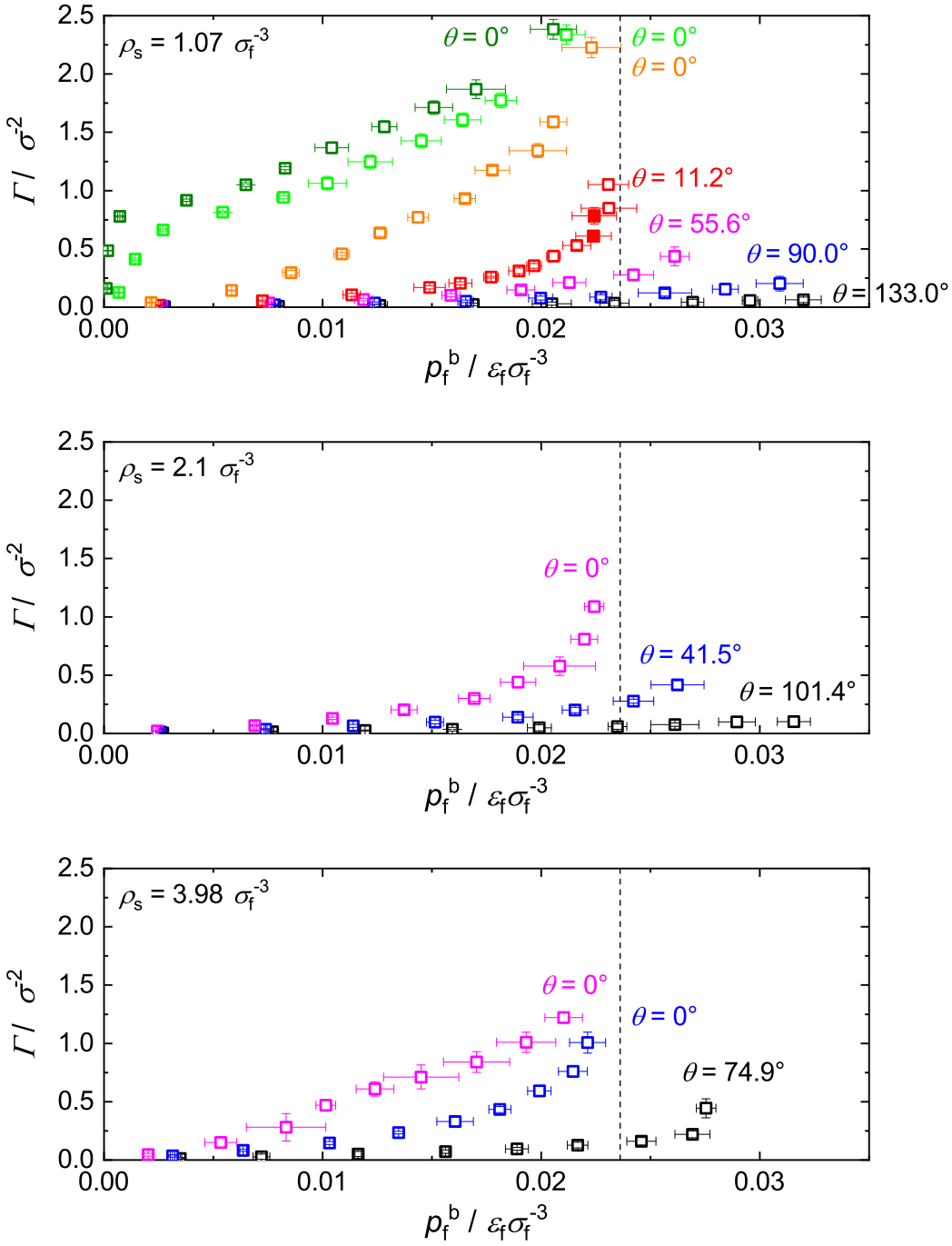

Figure 4: Adsorption isotherms for $T/T_c = 0.8$ and $\rho_s = 1.07\ \sigma_f^{-3}$ (top), $\rho_s = 2.1\ \sigma_f^{-3}$ (middle), and $\rho_s = 3.98\ \sigma_f^{-3}$ (bottom). The simulation data is shown as symbols, the uncertainty is indicated by error bars. The saturation pressure is shown as a black dashed line and the contact angle θ is reported for all adsorption isotherms. *Top:* $W = 1.08$ (black), $W = 1.58$ (blue), $W = 2.00$ (violet), $W = 2.31$ (red), $W = 3.08$ (orange), $W = 4.62$ (green), and $W = 6.16$ (dark green). The filled symbols in the top panel indicate a jump in the adsorption isotherm where prewetting occurs. *Middle:* $W = 1.69$ (black), $W = 2.48$ (blue), and $W = 3.14$ (violet). *Bottom:* $W = 2.83$ (black), $W = 4.15$ (blue), and $W = 5.25$ (violet). [This Figure is 2 columns wide]

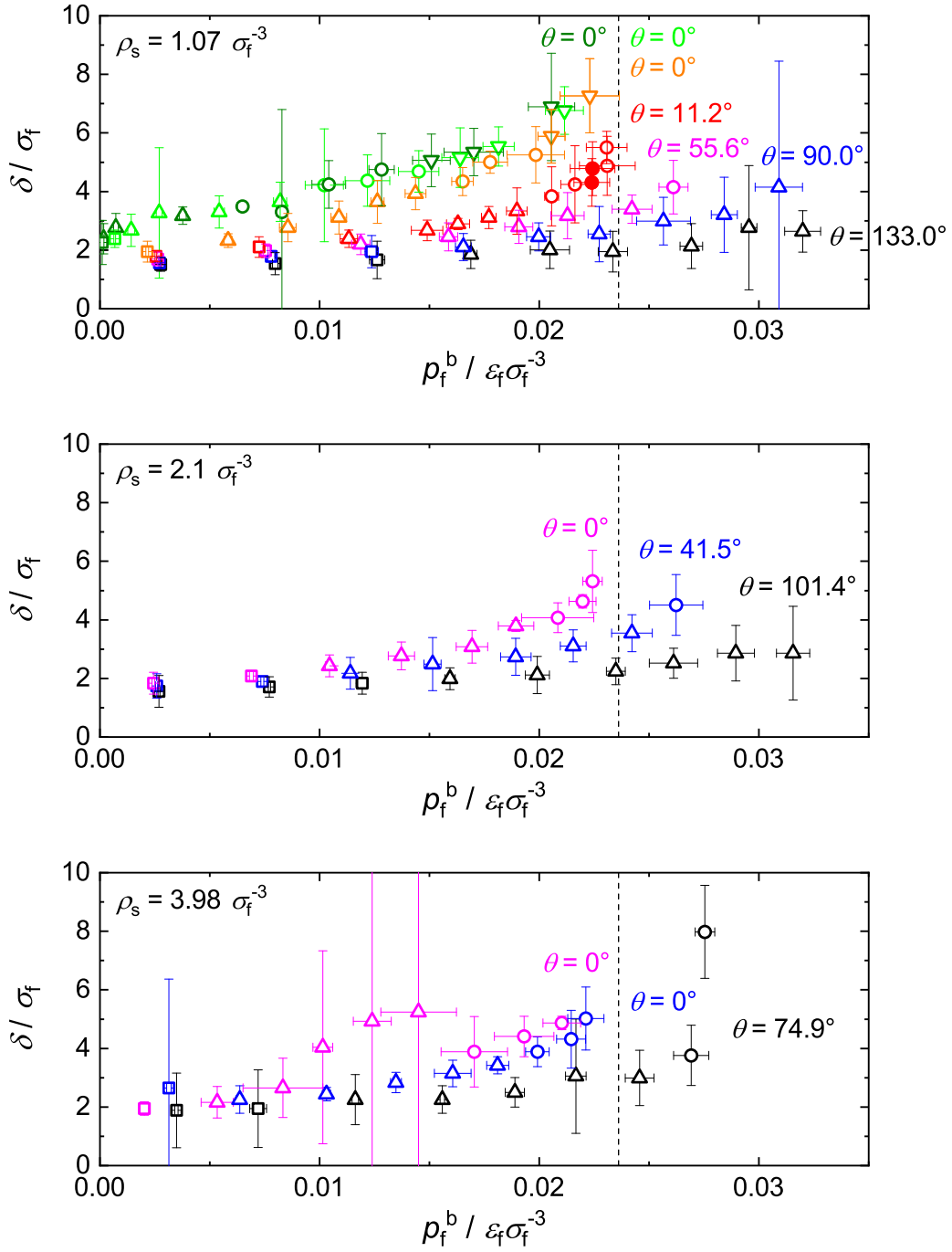

Figure 5: Adsorption layer thickness for $T/T_c = 0.8$ and $\rho_s = 1.07\ \sigma_f^{-3}$ (top), $\rho_s = 2.1\ \sigma_f^{-3}$ (middle), and $\rho_s = 3.98\ \sigma_f^{-3}$ (bottom). The simulation data is shown as symbols, the uncertainty is indicated by error bars. The number of peaks in the adsorption layer is shown with different symbols: one peak (□), two peaks (△), three peaks (◯), and four peaks (▽). The saturation pressure is shown as a black dashed line and the contact angle θ is reported for all W. *Top:* $W = 1.08$ (black), $W = 1.58$ (blue), $W = 2.00$ (violet), $W = 2.31$ (red), $W = 3.08$ (orange), $W = 4.62$ (green), and $W = 6.16$ (dark green). The filled symbols show a jump in the adsorption isotherm where prewetting occurs. *Middle:* $W = 1.69$ (black), $W = 2.48$ (blue), and $W = 3.14$ (violet). *Bottom:* $W = 2.83$ (black), $W = 4.15$ (blue), and $W = 5.25$ (violet). [This Figure is 2 columns wide]

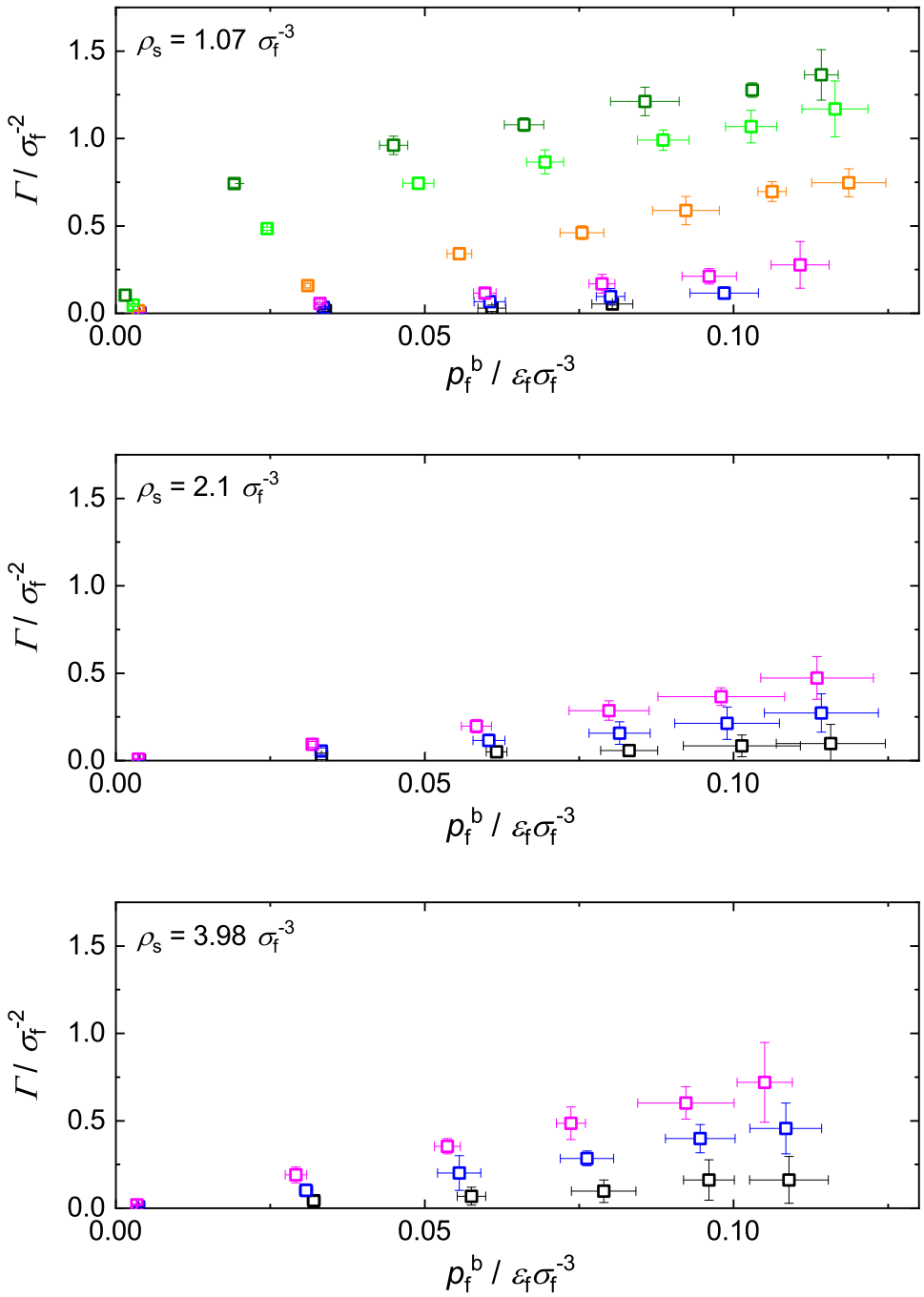

Figure 6: Adsorption isotherms for $T/T_c = 1.1$ and $\rho_s = 1.07\ \sigma_f^{-3}$ (top), $\rho_s = 2.1\ \sigma_f^{-3}$ (middle), and $\rho_s = 3.98\ \sigma_f^{-3}$ (bottom). The simulation data is shown as symbols, the uncertainty is indicated by error bars. *Top:* $W = 1.08$ (black), $W = 1.58$ (blue), $W = 2.00$ (violet), $W = 3.08$ (orange), $W = 4.62$ (green), and $W = 6.16$ (dark green). *Middle:* $W = 1.69$ (black), $W = 2.48$ (blue), and $W = 3.14$ (violet). *Bottom:* $W = 2.83$ (black), $W = 4.15$ (blue), and $W = 5.25$ (violet). [This Figure is 2 columns wide]

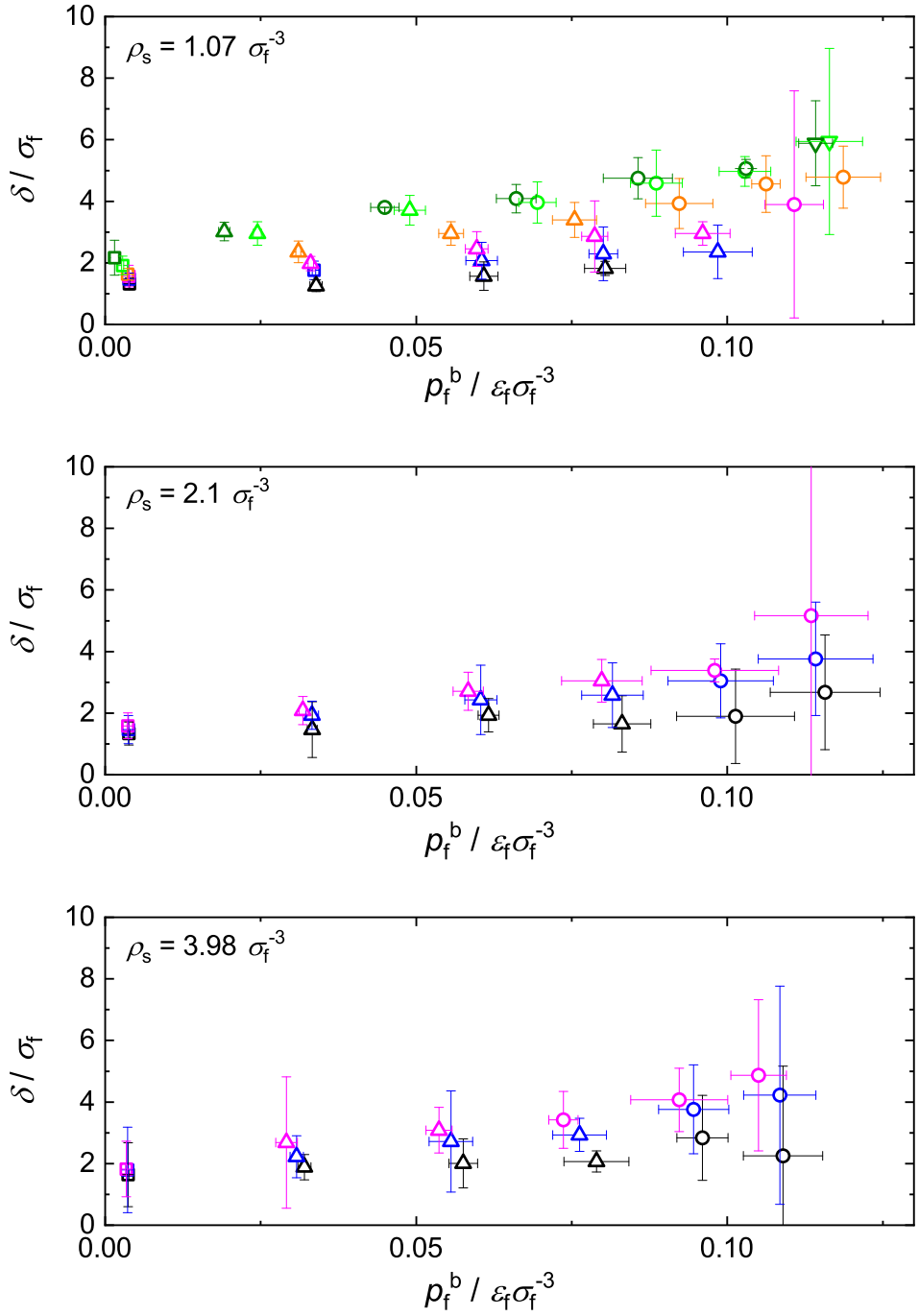

Figure 7: Adsorption layer thickness for $T/T_c = 1.1$ and $\rho_s = 1.07\ \sigma_f^{-3}$ (top), $\rho_s = 2.1\ \sigma_f^{-3}$ (middle), and $\rho_s = 3.98\ \sigma_f^{-3}$ (bottom). The simulation data is shown as symbols, the uncertainty is indicated by error bars. The number of peaks in the adsorption layer is shown with different symbols: one peak (□), two peaks (△), three peaks (◯), and four peaks (▽). *Top:* $W = 1.08$ (black), $W = 1.58$ (blue), $W = 2.00$ (violet), $W = 3.08$ (orange), $W = 4.62$ (green), and $W = 6.16$ (dark green). *Middle:* $W = 1.69$ (black), $W = 2.48$ (blue), and $W = 3.14$ (violet). *Bottom:* $W = 2.83$ (black), $W = 4.15$ (blue), and $W = 5.25$ (violet). [This Figure is 2 columns wide]

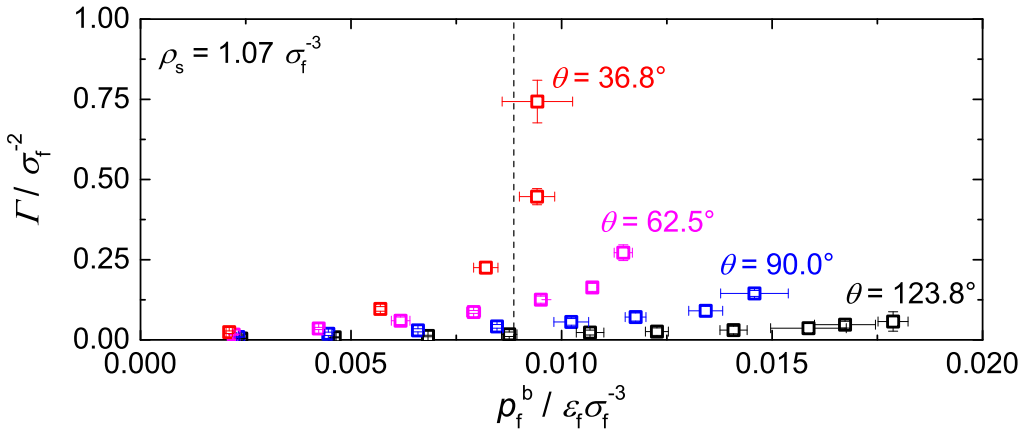

Figure 8: Adsorption isotherms for $T/T_c = 0.7$ and $\rho_s = 1.07\ \sigma_f^{-3}$. $W = 1.08$ (black), $W = 1.58$ (blue), $W = 2.00$ (violet), and $W = 2.31$ (red). The simulation data is shown as symbols, the uncertainty is indicated by error bars. The saturation pressure is shown as a black dashed line and the contact angle θ is reported for all adsorption isotherms. [This Figure is 2 columns wide]

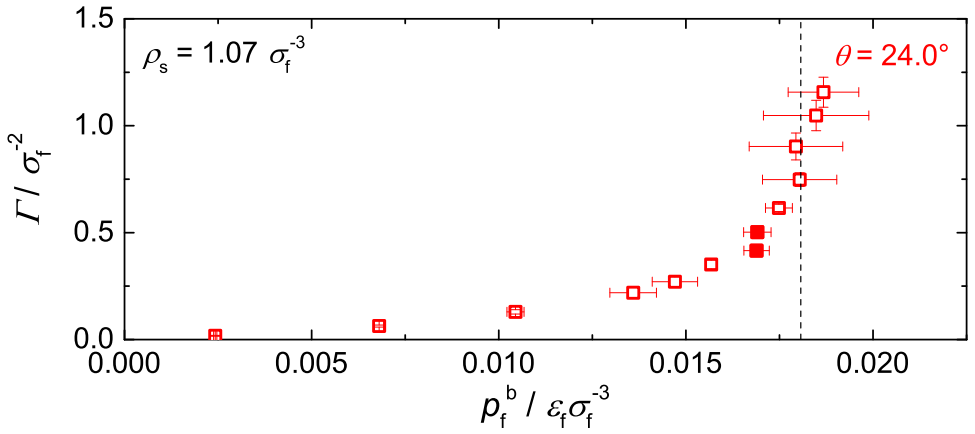

Figure 9: Adsorption isotherms for $T/T_c = 0.77$ and $\rho_s = 1.07\ \sigma_f^{-3}$. $W = 2.31$ (red). The simulation data is shown as symbols, the uncertainty is indicated by error bars. The saturation pressure is shown as a black dashed line and the contact angle θ is reported for the adsorption isotherm. The filled symbols show a jump in the adsorption isotherm where prewetting occurs. [This Figure is 2 columns wide]

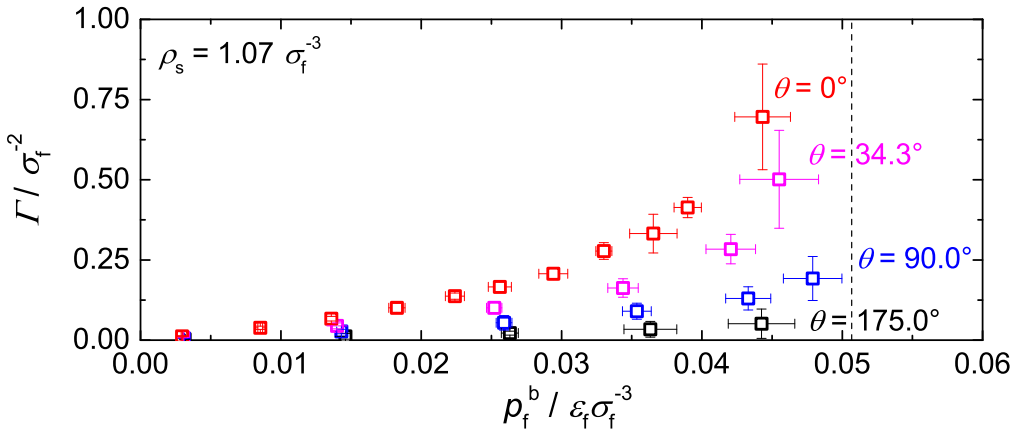

Figure 10: Adsorption isotherms for $T/T_c = 0.9$ and $\rho_s = 1.07\ \sigma_f^{-3}$. $W = 1.08$ (black), $W = 1.58$ (blue), $W = 2.00$ (violet), and $W = 2.31$ (red). The simulation data is shown as symbols, the uncertainty is indicated by error bars. The saturation pressure is shown as a black dashed line and the contact angle θ is reported for all adsorption isotherms. [This Figure is 2 columns wide]

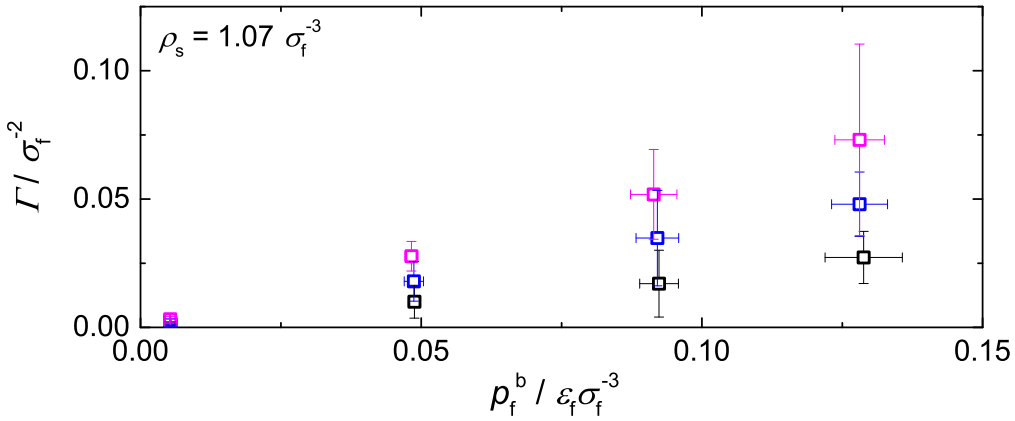

Figure 11: Adsorption isotherms for $T/T_c = 1.5$ and $\rho_s = 1.07\ \sigma_f^{-3}$. $W = 1.08$ (black), $W = 1.58$ (blue), and $W = 2.00$ (violet). The simulation data is shown as symbols, the uncertainty is indicated by error bars. [This Figure is 2 columns wide]

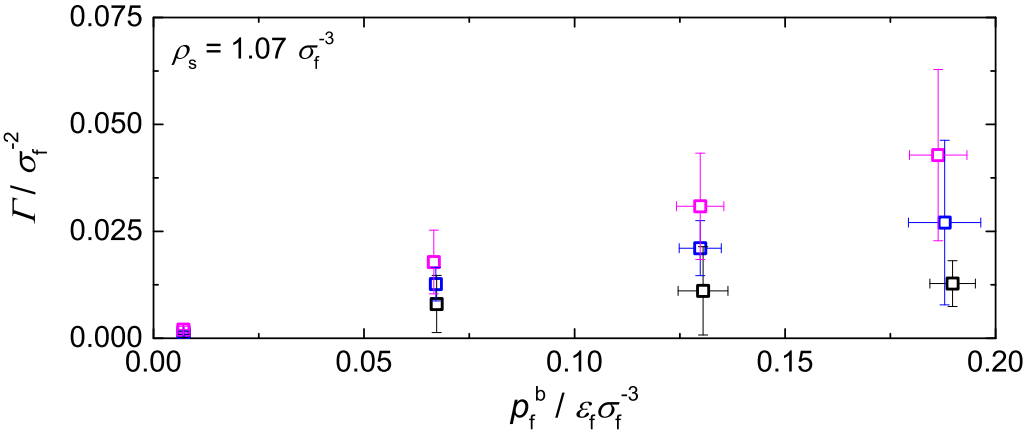

Figure 12: Adsorption isotherms for $T/T_c = 2.0$ and $\rho_s = 1.07\ \sigma_f^{-3}$. $W = 1.08$ (black), $W = 1.58$ (blue), and $W = 2.00$ (violet). The simulation data is shown as symbols, the uncertainty is indicated by error bars. [This Figure is 2 columns wide]

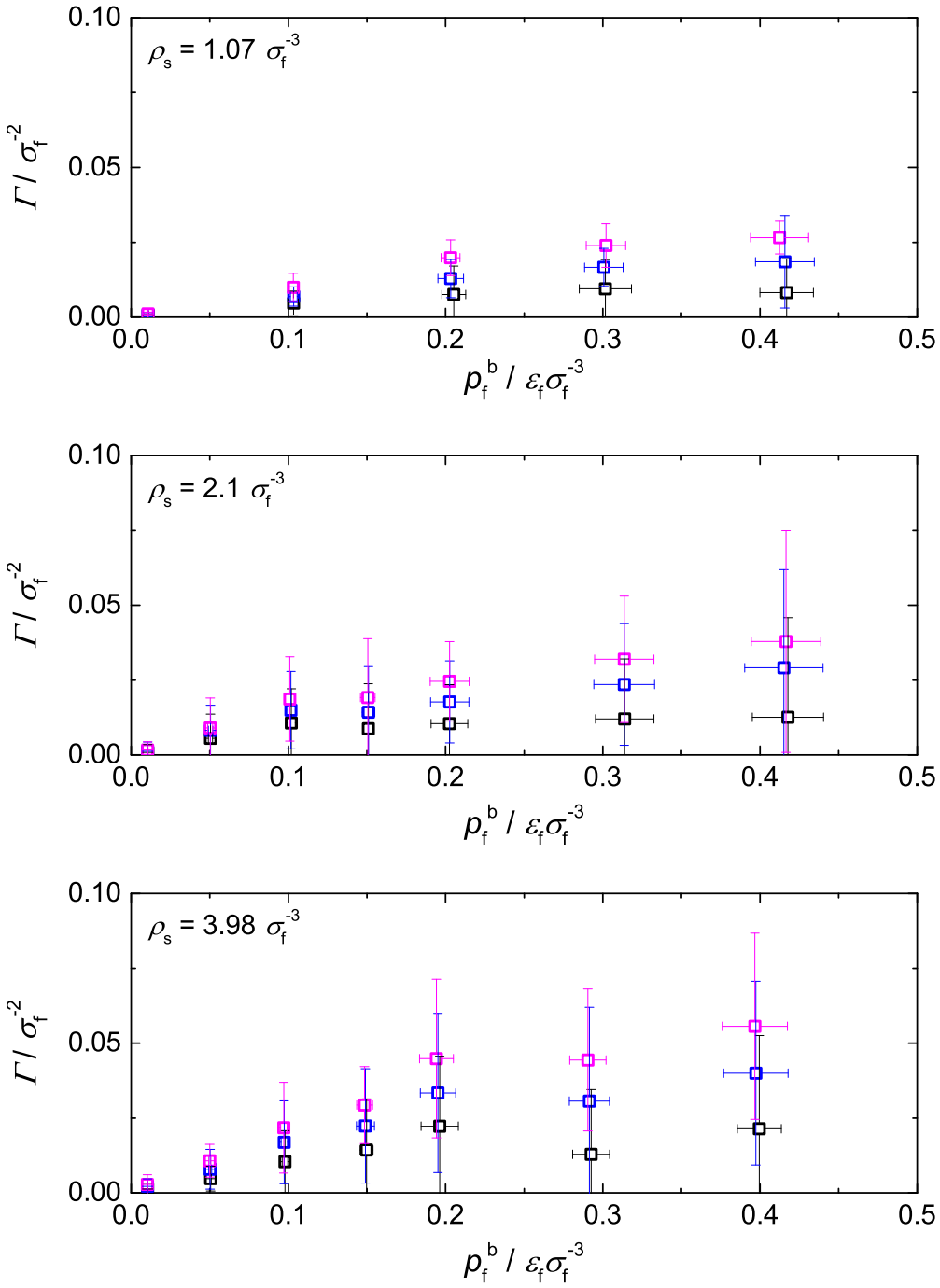

Figure 13: Adsorption isotherms for $T/T_c = 3.0$ and $\rho_s = 1.07\ \sigma_f^{-3}$ (top), $\rho_s = 2.1\ \sigma_f^{-3}$ (middle), and $\rho_s = 3.98\ \sigma_f^{-3}$ (bottom). The simulation data is shown as symbols, the uncertainty is indicated by error bars. *Top:* $W = 1.08$ (black), $W = 1.58$ (blue), $W = 2.00$ (violet). *Middle:* $W = 1.69$ (black), $W = 2.48$ (blue), and $W = 3.14$ (violet). *Bottom:* $W = 2.83$ (black), $W = 4.15$ (blue), and $W = 5.25$ (violet). [This Figure is 2 columns wide]

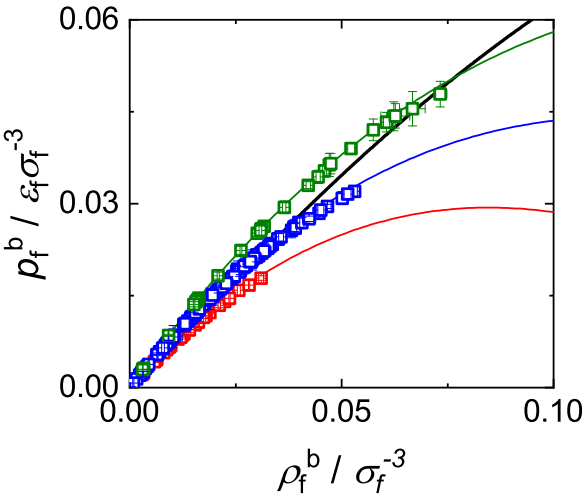

Figure 14: Bulk pressure versus density for the LJTS fluid with $r_c = 2.5\ \sigma_f$ calculated with the PeTS EOS[5] (lines) on the vapor side. The binodal is shown as black solid line and the isotherms for $T/T_c = 0.7$, 0.8, and 0.9 as red, blue, and green line. The bulk pressures of the adsorption simulations are shown as symbols, red for $T/T_c = 0.7$, blue for $T/T_c = 0.8$ green for $T/T_c = 0.9$. [This Figure is 1 column wide]

Molecular Dynamics Study of Adsorption of the Lennard-Jones Truncated and Shifted Fluid on Planar Walls

Michaela Heier,[†] Felix Diewald,[‡] Martin T. Horsch,[†,¶] Kai Langenbach,[*,†] Ralf Müller,[‡] and Hans Hasse[†]

[†]*Laboratory of Engineering Thermodynamics, Technische Universität Kaiserslautern, Kaiserslautern, Germany*

[‡]*Institute of Applied Mechanics, Technische Universität Kaiserslautern, Kaiserslautern, Germany*

[¶]*Current address: Scientific Computing Division, STFC Daresbury Laboratory, UK Research and Innovation, Warrington, United Kingdom*

E-mail: kai.langenbach@mv-uni-kl.de

Phone: +49 (0)631 2054685. Fax: +49 (0)631 2053835

Supplementary Information

Simulation Scenario

The simulation scenario contains an atomistic wall which is fixed at the bottom of the simulation box by a LJTS-9-3 potential with a cut-off radius of 2.5 σ_f. This potential is located at a height of $y = 0\ \sigma_\mathrm{f}$ and is defined as:

$$u_{\mathrm{LJ93}}(r) = \frac{4}{3}\pi\varepsilon_{\mathrm{ss}}\rho_{\mathrm{s}}\sigma_{\mathrm{ss}}^3\left[\frac{1}{15}\left(\frac{\sigma_{\mathrm{ss}}}{r}\right)^9 - \frac{1}{2}\left(\frac{\sigma_{\mathrm{ss}}}{r}\right)^3\right] \tag{1}$$

$$u_{\mathrm{LJTS93}}(r) = \begin{cases} u_{\mathrm{LJ93}}(r) - u_{\mathrm{LJ93}}(r_{\mathrm{c}}) & r \leq r_{\mathrm{c}} \\ 0 & r > r_{\mathrm{c}} \end{cases}. \tag{2}$$

Where $\varepsilon_{\mathrm{ss}}$ and σ_{ss} are the energy and size parameter of the solid-solid (ss) interaction and ρ_{s} the density of the atomistic wall. Due to its cut-off radius, this potential is acting only on the atomistic wall because the height of the atomistic wall is always bigger than 2.5 σ_{f}. At the top of the simulation box (at a height of $y = 55\ \sigma_{\mathrm{f}}$) a membrane is applied. It avoids the layer growth underneath the atomistic wall due to the periodic boundary conditions. Especially, when investigating adsorption at high pressures, a strong layer growth would occur at both sides of the wall. This would lead to a reduction of the amount of bulk vapor phase. The membrane avoids this layer growth by applying a reset force of F = -20·Δy, whereas Δy is the distance from the membrane to particles above the membrane.

Size Effects

To examine the influence of the amount of fluid particles N_{f} on the surface excess, simulations for several sets of parameters are performed. In these simulations the number of fluid particles and therefore the system size in x- and z-direction is changed. The simulations are carried out for a constant fluid density ρ_{f}. Table 1 gives an overview of the simulation conditions for which the size effect was studied.

[Table 1 near here]

The number of fluid particles varied between N_{f} = 1,931 and 9,155. The results of these simulations are shown in Figure 1 and Table 2.

[Figure 1 near here]

[Table 2 near here]

For $N_\mathrm{f} < 6{,}000$ finite size effects occur. Above $N_\mathrm{f} = 6{,}000$ the surface excess stays constant within the uncertainties.

Numerical simulation results

All results of the adsorption simulations for the surface excess and the adsorption layer thickness are given in Table 3. In the main article already all adsorption isotherms are shown. However, only selected adsorption layer thickness curves for $T/T_\mathrm{c} = 0.8$ and $T/T_\mathrm{c} = 1.1$. In Figure 3, 4, and 5 the remaining ones are shown.

[Figure 3 near here.]

[Figure 4 near here.]

[Figure 5 near here.]

As already mentioned in the article, the curvature of the layer thickness is the same than the curvature of the adsorption isotherms. For $T/T_\mathrm{c} = 0.77$ a jump in the layer thickness at the wetting transition occurs. The results, discussed in the article, also apply to the results shown here.

Detection of Droplet Growth in the Metastable Region

For an increasing supersaturation of the vapor phase a droplet growth at the surface was observed. This is indicated by a decrease in the bulk fluid pressure and a droplet-like layer-

ing in a density profile averaged in z-direction $\rho_{\mathrm{f}}(x, y)$. Figure 2 shows such a mean density profile with droplet growth.

[Figure 2 near here]

The colors show the values of the fluid density. The first adsorption layer on the wall is continuous whereas the higher layers only occur in some areas. This indicates a droplet growth. When a decrease in the bulk fluid pressure or a droplet growth in the mean density profile $\rho_{\mathrm{f}}^{*}(x, y)$ is observed no adsorption is calculated.

Tables

Table 1: Overview of simulation conditions for studying the size effect.

$T/\varepsilon_\mathrm{f}k^{-1}$	$\rho_\mathrm{s}/\sigma_\mathrm{f}^{-3}$	ζ
0.7	1.07	0.35
		0.65
0.8	1.07	0.35
		0.65

Table 2: Simulation results for testing the influence of the number of particles N_f on the surface excess Γ for $T = 0.7$, 0.8, and 0.9 ε_f/k and $\zeta = 0.35$ and 0.65. The number in parentheses indicates the statistical uncertainty in the last decimal digit.

$T/\varepsilon_\mathrm{f}k^{-1}$	ζ	$\Gamma/\sigma_\mathrm{f}^{-2}$	N_f
0.7	0.35	0.018(12)	1931
		0.015(5)	3213
		0.0146(47)	4255
		0.0139(31)	6078
		0.0143(20)	7846
		0.0142(34)	9155
	0.65	0.095(25)	1931
		0.085(9)	3213
		0.084(7)	4255
		0.083(13)	6078
		0.086(5)	7846
		0.085(5)	9155
0.8	0.35	0.013(13)	1931
		0.011(6)	3213
		0.0097(46)	4255
		0.009(6)	5227
		0.0106(37)	6916
		0.0116(37)	8622
	0.65	0.057(20)	1931
		0.0427(45)	3213
		0.0446(42)	4255
		0.046(6)	5227
		0.047(5)	6916
		0.0485(47)	8622

Table 3: Bulk fluid density $\rho_{\mathrm{f}}^{\mathrm{b}}$, bulk fluid pressure $p_{\mathrm{f}}^{\mathrm{b}}$, surface excess Γ, layer thickness δ, and number of adsorption layer peaks N_{peaks} for the adsorption simulations for changing temperature T, solid density ρ_{s}, and reduced solid-fluid interaction energy ζ.

T/T_{c}	$\rho_{\mathrm{s}}/\sigma_{\mathrm{f}}^{-3}$	ζ	$\rho_{\mathrm{f}}^{\mathrm{b}}/\sigma_{\mathrm{f}}^{-3}$	$p_{\mathrm{f}}^{\mathrm{b}}/\varepsilon\sigma_{\mathrm{f}}^{-3}$	$\Gamma/\sigma_{\mathrm{f}}^{-2}$	$\delta/\sigma_{\mathrm{f}}$	N_{peaks}
0.7	1.07	0.35	0.003243(14)	0.002394(39)	0.0043(7)	1.51(23)	1
			0.006404(30)	0.004611(34)	0.0080(15)	1.57(35)	1
			0.00971(5)	0.00683(11)	0.0122(23)	1.70(23)	1
			0.01281(14)	0.00876(18)	0.018(7)	1.9(6)	1
			0.01609(10)	0.01068(33)	0.023(8)	1.92(42)	1
			0.01894(14)	0.01226(27)	0.026(12)	2.0(5)	2
			0.02241(24)	0.01408(32)	0.031(12)	2.04(35)	2
			0.02574(37)	0.0159(9)	0.037(18)	2.1(8)	2
			0.02814(14)	0.0167(7)	0.048(11)	2.5(6)	2
			0.0310(6)	0.01787(36)	0.057(30)	3.0(31)	2
		0.514	0.003146(20)	0.002323(39)	0.0090(10)	1.66(23)	1
			0.00618(10)	0.00446(9)	0.019(5)	1.85(48)	1
			0.00934(10)	0.00659(12)	0.0298(48)	2.04(35)	1
			0.01229(8)	0.00847(11)	0.042(6)	2.14(23)	1
			0.01540(18)	0.01023(41)	0.056(19)	2.23(52)	2
			0.01801(29)	0.01176(25)	0.071(12)	2.39(30)	2
			0.02111(28)	0.01342(40)	0.090(14)	2.6(7)	2
			0.02354(17)	0.0146(8)	0.145(9)	4.3(14)	2
		0.65	0.002991(36)	0.002213(31)	0.0167(19)	1.85(38)	1
			0.00585(6)	0.00423(9)	0.0356(36)	2.07(30)	1
			0.00874(23)	0.00618(22)	0.060(11)	2.3(6)	1
			0.01140(12)	0.00791(16)	0.0870(45)	2.42(46)	1
			0.01404(14)	0.00951(13)	0.125(11)	2.80(48)	2
			0.01618(28)	0.01073(11)	0.164(13)	2.92(38)	2
			0.01743(49)	0.01147(22)	0.272(25)	4.2(26)	2
		0.75	0.00284(8)	0.00211(7)	0.0239(40)	1.92(30)	1
			0.00800(11)	0.00570(14)	0.097(7)	2.4(7)	1
			0.01199(40)	0.00820(29)	0.225(19)	2.95(23)	2
			0.0139(5)	0.00942(42)	0.446(25)	3.62(35)	2
			0.0140(13)	0.0094(8)	0.74(6)	4.6(6)	3
0.77	1.07	0.75	0.002968(40)	0.002424(45)	0.0178(20)	1.79(19)	1
			0.00866(10)	0.00680(12)	0.0632(47)	2.17(38)	1
			0.01391(19)	0.01045(23)	0.130(10)	2.6(6)	2
			0.0185(5)	0.0136(6)	0.219(25)	3.90(38)	2
			0.02025(45)	0.0147(6)	0.270(23)	3.1(6)	2
			0.02191(41)	0.01568(14)	0.351(19)	3.43(48)	2
			0.02384(31)	0.01689(34)	0.416(15)	3.7(7)	2
			0.02403(39)	0.01691(37)	0.503(20)	3.96(30)	3
			0.02506(33)	0.01749(36)	0.616(17)	4.3(6)	3
			0.0255(6)	0.0180(10)	0.748(32)	4.5(6)	3
			0.0258(13)	0.0179(12)	0.90(6)	5.0(11)	3
			0.0265(15)	0.0185(14)	1.05(7)	5.2(7)	3
			0.0269(14)	0.0187(9)	1.16(7)	5.6(6)	3
0.8	1.07	0.35	0.003263(20)	0.002770(37)	0.0032(10)	1.51(23)	1
			0.00976(9)	0.00798(13)	0.0092(41)	1.54(38)	1

			0.01622(16)	0.01262(35)	0.015(11)	1.7(6)	1
			0.02253(20)	0.01688(28)	0.023(10)	1.85(48)	2
			0.02850(16)	0.0205(9)	0.030(13)	2.0(6)	2
			0.03362(46)	0.0234(7)	0.033(24)	1.9(7)	2
			0.0399(5)	0.0269(5)	0.041(27)	2.1(8)	2
			0.0467(8)	0.02955(36)	0.057(39)	2.8(21)	2
			0.0531(6)	0.0320(8)	0.064(23)	2.6(7)	2
		0.514	0.003193(15)	0.002709(33)	0.0067(7)	1.57(19)	1
			0.00952(9)	0.00780(16)	0.021(4)	1.79(19)	1
			0.01582(17)	0.01237(31)	0.035(10)	1.9(6)	1
			0.02196(14)	0.01654(36)	0.051(11)	2.11(46)	2
			0.02755(27)	0.0200(5)	0.078(16)	2.45(48)	2
			0.03251(45)	0.0227(5)	0.086(23)	2.5(9)	2
			0.0382(6)	0.0257(12)	0.123(28)	3.0(8)	2
			0.0447(10)	0.0284(6)	0.16(5)	3.2(13)	2
			0.0502(14)	0.0309(11)	0.20(6)	4.2(43)	2
		0.65	0.003099(22)	0.002632(47)	0.0113(11)	1.70(23)	1
			0.00919(12)	0.00754(12)	0.037(7)	1.98(23)	1
			0.01522(14)	0.01187(42)	0.065(9)	2.20(35)	2
			0.02091(12)	0.01587(42)	0.102(14)	2.45(48)	2
			0.0261(6)	0.0191(6)	0.149(30)	2.8(6)	2
			0.0300(9)	0.0213(8)	0.212(41)	3.2(8)	2
			0.0351(9)	0.0242(9)	0.277(43)	3.40(48)	2
			0.0389(16)	0.0261(7)	0.44(8)	4.2(9)	3
		0.75	0.002998(27)	0.00255(42)	0.0162(14)	1.79(19)	1
			0.00883(14)	0.00725(18)	0.055(7)	2.11(35)	1
			0.01438(26)	0.01133(39)	0.106(12)	2.39(30)	2
			0.01948(27)	0.0149(7)	0.170(14)	2.67(35)	2
			0.02157(28)	0.0163(5)	0.205(14)	2.89(19)	2
			0.02379(17)	0.01770(33)	0.258(8)	3.11(38)	2
			0.02594(48)	0.01898(47)	0.312(24)	3.3(8)	2
			0.02701(46)	0.01967(34)	0.355(20)	3.5(6)	2
			0.0286(7)	0.02056(32)	0.438(38)	3.8(10)	3
			0.0299(6)	0.0216(6)	0.529(32)	4.2(13)	3
			0.03168(35)	0.0224(8)	0.610(17)	4,3(8)	3
			0.0319(14)	0.0224(10)	0.78(7)	4.8(9)	3
			0.0331(8)	0.0231(13)	0.849(39)	4.9(10)	3
			0.0329(9)	0.0231(9)	1.052(46)	5.5(6)	3
		1.0	0.00253(7)	0.00215(6)	0.0394(34)	1.95(35)	1
			0.00703(9)	0.00584(18)	0.1439(39)	2.33(23)	2
			0.01055(39)	0.00855(38)	0.296(20)	2.77(48)	2
			0.01373(17)	0.01088(35)	0.457(12)	3.1(6)	2
			0.0162(5)	0.01263(30)	0.638(30)	3.6(7)	2
			0.0186(10)	0.01436(47)	0.771(48)	3.9(6)	2
			0.0218(6)	0.0165(5)	0.931(30)	4.34(48)	3
			0.0240(7)	0.0178(8)	1.175(33)	5.00(38)	3
			0.0270(12)	0.0198(13)	1.34(6)	5.3(10)	3
			0.0284(11)	0.0206(6)	1.59(5)	5.9(9)	4
			0.0316(17)	0.0223(13)	2.23(9)	7.3(13)	4
		1.5	0.000784(40)	0.000674(39)	0.1265(20)	2.39(30)	1
			0.00166(18)	0.00142(16)	0.412(9)	2.7(6)	2

		0.00318(16)	0.00270(14)	0.663(8)	3.3(22)	2
		0.00655(16)	0.00543(23)	0.815(10)	3.3(6)	2
		0.01007(26)	0.00820(30)	0.942(13)	3.6(7)	2
		0.0128(12)	0.0102(9)	1.06(6)	4.2(19)	3
		0.0155(12)	0.0122(10)	1.25(6)	4.4(9)	3
		0.0189(12)	0.0145(9)	1.43(6)	4.7(7)	3
		0.0217(12)	0.0164(8)	1.61(6)	5.2(10)	4
		0.0247(13)	0.0182(7)	1.77(6)	5.5(7)	4
		0.0294(18)	0.0212(9)	2.34(8)	6.8(8)	4
	2.0	0.00012(10)	0.00010(8)	0.160(5)	2.3(8)	1
		0.000192(29)	0.000165(24)	0.4856(14)	2.4(5)	2
		0.00085(13)	0.00073(10)	0.780(7)	2.77(48)	2
		0.00449(16)	0.00377(16)	0.917(10)	3.18(30)	2
		0.00789(32)	0.00649(24)	1.050(17)	3.48996(0)	3
		0.01022(26)	0.00828(26)	1.191(13)	3.3(35)	3
		0.0131(10)	0.0104(8)	1.367(49)	4.2(8)	3
		0.0165(10)	0.0128(6)	1.55(5)	4.7(12)	3
		0.0196(12)	0.0151(9)	1.71(6)	5.1(9)	4
		0.0228(16)	0.0170(13)	1.87(8)	5.3(8)	4
		0.0285(17)	0.0206(11)	2.38(8)	6.9(18)	4
2.1	0.35	0.003165(47)	0.002683(45)	0.0053(24)	1.6(5)	1
		0.00943(7)	0.007714(48)	0.0151(39)	1.71(35)	1
		0.01520(8)	0.01194(27)	0.0258(40)	1.84(37)	1
		0.02093(25)	0.01594(23)	0.037(16)	1.99(37)	2
		0.02748(43)	0.0199(5)	0.049(26)	2.1(6)	2
		0.03330(46)	0.02348(43)	0.059(23)	2.24(46)	2
		0.03897(36)	0.0261(11)	0.076(14)	2.5(5)	2
		0.0451(7)	0.0290(8)	0.099(43)	2.9(10)	2
		0.0514(8)	0.0316(8)	0.101(44)	2.9(16)	2
	0.514	0.003034(45)	0.00258(5)	0.0119(24)	1.74(42)	1
		0.00902(8)	0.00739(7)	0.0353(39)	1.89841(0)	1
		0.01442(23)	0.01140(21)	0.065(13)	2.2(5)	2
		0.01975(29)	0.01514(39)	0.098(16)	2.5(9)	2
		0.02566(29)	0.0189(7)	0.139(20)	2.7(6)	2
		0.03046(45)	0.0215(6)	0.201(23)	3.1(5)	2
		0.03492(26)	0.0242(9)	0.277(17)	3.5(6)	2
		0.0388(7)	0.0262(12)	0.417(37)	4.5(10)	3
		0.0390(14)	0.0260(8)	0.72(8)	8.2(12)	3
	0.65	0.00288(6)	0.00244(6)	0.0214(32)	1.84(37)	1
		0.00837(10)	0.00690(9)	0.068(5)	2.08(19)	1
		0.01314(18)	0.01045(20)	0.130(10)	2.43(37)	2
		0.0176(6)	0.0137(6)	0.203(32)	2.77(48)	2
		0.02247(40)	0.0169(7)	0.301(23)	3.1(6)	2
		0.0257(9)	0.0189(8)	0.441(43)	3.79(19)	2
		0.0289(16)	0.0208(16)	0.58(8)	4.1(5)	3
		0.0310(10)	0.0220(6)	0.809(41)	4.63(23)	3
		0.0318(10)	0.02243(44)	1.088(47)	5.3(11)	3
3.98	0.35	0.00415(14)	0.00349(7)	0.013(8)	1.9(13)	1
		0.00879(39)	0.00720(38)	0.028(22)	1.9(13)	1
		0.01467(31)	0.01163(14)	0.052(23)	2.3(9)	2
		0.02047(23)	0.01559(10)	0.076(13)	2.25(47)	2

			0.02589(18)	0.01889(43)	0.098(11)	2.5(5)	2
			0.0302(5)	0.02167(47)	0.128(25)	3.1(19)	2
			0.0357(6)	0.0246(7)	0.167(31)	3.0(9)	2
			0.0406(5)	0.0269(8)	0.220(30)	3.8(10)	3
			0.0423(16)	0.02754(45)	0.44(8)	8.0(16)	3
		0.514	0.00372(16)	0.00314(10)	0.035(9)	2.7(37)	1
			0.00772(18)	0.00637(16)	0.083(9)	2.25(47)	2
			0.01283(17)	0.01031(19)	0.146(13)	2.44(23)	2
			0.01731(24)	0.01348(25)	0.235(11)	2.84(35)	2
			0.0213(7)	0.0161(8)	0.329(36)	3.15(45)	2
			0.0243(5)	0.0181(5)	0.433(27)	3.42(29)	2
			0.0273(8)	0.0199(5)	0.594(43)	3.9(5)	3
			0.0300(9)	0.0215(7)	0.759(46)	4.3(10)	3
			0.0313(18)	0.0221(8)	1.01(9)	5.0(11)	3
		0.65	0.00237(23)	0.00202(19)	0.046(12)	1.95(23)	1
			0.0064(9)	0.0053(7)	0.149(46)	2.2(5)	2
			0.0102(22)	0.0083(18)	0.28(12)	2.7(10)	2
			0.0128(8)	0.01014(45)	0.471(46)	4.0(33)	2
			0.0160(11)	0.0124(9)	0.61(6)	5(8)	2
			0.0189(20)	0.0145(17)	0.71(10)	5(9)	2
			0.0225(17)	0.0170(15)	0.84(9)	3,9(12)	3
			0.0255(17)	0.0193(14)	1.01(9)	4.4(7)	3
			0.0289(9)	0.0210(9)	1.222(48)	4.87(23)	3
0.9	1.07	0.35	0.003292(26)	0.00315(5)	0.0028(13)	1.44(30)	1
			0.01630(16)	0.01460(39)	0.012(9)	1.4(5)	1
			0.03170(21)	0.0263(6)	0.022(6)	1.57(19)	2
			0.04710(41)	0.0363(19)	0.034(25)	1.8(10)	2
			0.0623(9)	0.0442(24)	0.051(46)	2.2(18)	2
		0.514	0.003240(10)	0.00309(5)	0.0054(5)	1.51(23)	1
			0.015974(6)	0.01431(33)	0.027(7)	1.79(35)	1
			0.03105(43)	0.0259(6)	0.054(23)	2.04(35)	2
			0.04592(43)	0.0354(10)	0.090(25)	2.5(6)	2
			0.0606(7)	0.0433(16)	0.130(36)	2.9(8)	2
			0.0733(16)	0.0479(21)	0.19(7)	3.6(14)	2
		0.65	0.003173(24)	0.003035(44)	0.0087(12)	1.66(23)	1
			0.01561(13)	0.01400(40)	0.044(9)	1.95(35)	1
			0.03010(31)	0.0252(5)	0.101(18)	2.42(46)	2
			0.04445(49)	0.0344(11)	0.162(29)	2.7(5)	2
			0.0575(11)	0.0421(18)	0.284(46)	3.7(8)	2
			0.0667(30)	0.0455(28)	0.50(15)	5.0(15)	3
		0.75	0.003083(37)	0.00296(6)	0.0120(19)	1.73(35)	1
			0.00916(10)	0.00853(17)	0.038(5)	1.92(30)	1
			0.01518(15)	0.01359(42)	0.067(7)	2.11(19)	1
			0.02087(28)	0.0183(6)	0.101(14)	2.3(6)	2
			0.02623(21)	0.0224(7)	0.137(10)	2.64(38)	2
			0.03084(30)	0.0256(8)	0.166(15)	2.7(6)	2
			0.03647(41)	0.0294(10)	0.207(18)	3.0(6)	2
			0.0421(5)	0.0330(6)	0.278(26)	3.3(8)	2
			0.0474(12)	0.0365(17)	0.33(6)	3.5(10)	2
			0.0522(8)	0.0390(10)	0.414(32)	3.7(10)	2

			0.0627(34)	0.0443(20)	0.70(16)	5.0(14)	3
1.1	1.07	0.35	0.003311(23)	0.00388(6)	0.0019(11)	1.32(19)	1
			0.03173(10)	0.0339(10)	0.0166(48)	1.26(19)	2
			0.06245(33)	0.0609(23)	0.029(19)	1.57(46)	2
			0.0909(7)	0.0804(33)	0.053(5)	1.82(23)	2
		0.514	0.003273(21)	0.00384(6)	0.0036(11)	1.48(19)	1
			0.03135(12)	0.03356(26)	0.034(5)	1.76(30)	1
			0.0616(6)	0.0605(25)	0.067(29)	2.1(6)	2
			0.0898(7)	0.0801(23)	0.097(45)	2.3(9)	2
			0.1210(8)	0.098(6)	0.116(34)	2.4(9)	2
		0.65	0.003232(26)	0.00379(6)	0.0057(13)	1.57(35)	1
			0.03090(11)	0.03305(43)	0.056(5)	1.98(23)	2
			0.0606(6)	0.0597(18)	0.115(24)	2.5(6)	2
			0.0883(7)	0.0787(21)	0.17(5)	2.9(12)	2
			0.1190(9)	0.0961(44)	0.212(44)	2.95(38)	2
			0.1492(24)	0.1108(47)	0.28(13)	3.9(37)	3
		1.0	0.003050(23)	0.003596(26)	0.0146(12)	1.63(19)	1
			0.02881(25)	0.03104(38)	0.158(13)	2.36(35)	2
			0.0560(5)	0.0556(20)	0.341(28)	2.95(38)	2
			0.0823(7)	0.0754(35)	0.461(39)	3.4(6)	2
			0.1113(16)	0.092(5)	0.59(8)	3.9(8)	3
			0.1403(16)	0.1062(23)	0.70(6)	4.6(9)	3
			0.1713(21)	0.119(6)	0.75(8)	4.8(10)	3
		1.5	0.00238(16)	0.00281(18)	0.048(8)	1.92(30)	1
			0.02224(18)	0.0245(7)	0.484(9)	2.95(38)	2
			0.0478(7)	0.0490(25)	0.744(33)	3.71(48)	2
			0.0740(13)	0.0695(30)	0.87(7)	4.0(7)	3
			0.1029(14)	0.0886(42)	0.99(6)	4.6(11)	3
			0.1324(17)	0.1028(41)	1.07(9)	4.97(48)	3
			0.1624(28)	0.116(5)	1.17(16)	5.9(30)	4
		2.0	0.0013(6)	0.0015(7)	0.104(28)	2.2(6)	1
			0.01706(43)	0.0191(9)	0.743(21)	3.02(30)	2
			0.0434(10)	0.0449(23)	0.96(5)	3.80468(0)	3
			0.0697(7)	0.0661(32)	1.079(39)	4.09(46)	3
			0.0985(13)	0.086(6)	1.21(8)	4.7(7)	3
			0.1281(18)	0.1030(10)	1.277(41)	5.06(30)	3
			0.1582(18)	0.1142(27)	1.36(14)	5.9(14)	4
	2.1	0.35	0.00324(6)	0.00380(13)	0.0024(31)	1.34(37)	1
			0.03093(33)	0.0333(8)	0.025(18)	1.5(9)	2
			0.06192(49)	0.0616(17)	0.050(32)	1.9(5)	2
			0.0934(7)	0.0831(46)	0.057(32)	1.6(9)	2
			0.1241(10)	0.101(9)	0.08(6)	1.9(15)	3
			0.1568(15)	0.116(9)	0.10(11)	2.7(19)	3
		0.514	0.00318(5)	0.00375(12)	0.0051(29)	1.46(46)	1
			0.03035(32)	0.0332(10)	0.055(18)	1.93(46)	2
			0.0606(5)	0.0604(26)	0.116(35)	2.4(11)	2
			0.0915(11)	0.0815(5)	0.16(6)	2.6(10)	2
			0.1215(8)	0.099(8)	0.21(9)	3.0(12)	3
			0.1533(15)	0.114(9)	0.27(11)	3.8(18)	3
		0.65	0.00311(6)	0.00366(13)	0.0089(30)	1.59(42)	1

			0.02958(30)	0.0318(6)	0.093(16)	2.08(46)	2
			0.0590(7)	0.0583(24)	0.197(39)	2.7(6)	2
			0.0889(9)	0.080(6)	0.29(6)	3.0(7)	2
			0.1184(6)	0.098(10)	0.37(5)	3.39(37)	3
			0.1490(20)	0.113(9)	0.47(12)	5(7)	3
	3.98	0.35	0.00316(7)	0.00371(10)	0.0053(37)	1.6(10)	1
			0.02979(45)	0.0320(10)	0.042(24)	1.88(41)	2
			0.0588(6)	0.0575(23)	0.07(5)	2.0(8)	2
			0.0883(13)	0.079(5)	0.097(64)	2.07(35)	2
			0.1176(19)	0.0960(41)	0.16(11)	2.8(14)	3
			0.1481(21)	0.109(6)	0.16(13)	2,3(29)	3
		0.514	0.00306(11)	0.00359(15)	0.010(6)	1.8(14)	1
			0.0286(7)	0.0308(11)	0.103(36)	2.2(7)	2
			0.0562(16)	0.0556(35)	0.20(10)	2.7(16)	2
			0.0848(7)	0.0763(43)	0.285(42)	2.9(5)	2
			0.1129(24)	0.095(6)	0.40(8)	3.8(14)	3
			0.1422(31)	0.108(6)	0.46(15)	4.2(35)	3
		0.65	0.00290(11)	0.00341(14)	0.019(6)	1.8(9)	1
			0.0269(9)	0.0292(17)	0.191(46)	2.7(21)	2
			0.0532(7)	0.0537(21)	0.355(43)	3.1(7)	2
			0.0808(19)	0.0737(24)	0.49(9)	3.4(9)	3
			0.1088(25)	0.092(8)	0.60(9)	4.1(10)	3
			0.1372(30)	0.1050(45)	0.72(23)	4.9(25)	3
1.5	1.07	0.35	0.003321(11)	0.00534(8)	0.0013(6)		
			0.03182(14)	0.0488(11)	0.010(6)		
			0.06254(27)	0.0924(35)	0.017(13)		
			0.09108(20)	0.129(7)	0.027(10)		
		0.514	0.003300(23)	0.00531(7)	0.0022(11)		
			0.03164(16)	0.0487(17)	0.018(8)		
			0.06218(17)	0.0921(38)	0.035(19)		
			0.09051(39)	0.128(5)	0.048(13)		
		0.65	0.003279(22)	0.00528(9)	0.0032(11)		
			0.03143(11)	0.0482(11)	0.028(6)		
			0.06177(32)	0.0914(41)	0.052(17)		
			0.0899(6)	0.1281(44)	0.073(37)		
			0.1212(7)	0.168(7)	0.077(21)		
2.0	1.07	0.35	0.003325(14)	0.00716(8)	0.0009(7)		
			0.03182(13)	0.0672(12)	0.008(7)		
			0.06254(18)	0.131(6)	0.011(10)		
			0.0911(5)	0.190(5)	0.013(5)		
		0.514	0.003314(8)	0.00713(9)	0.00145(46)		
			0.03172(7)	0.0671(12)	0.0127(39)		
			0.06231(19)	0.130(5)	0.021(6)		
			0.09076(39)	0.188(9)	0.027(19)		
			0.1219(6)	0.253(12)	0.031(22)		
		0.65	0.003301(15)	0.00710(9)	0.0020(8)		
			0.03161(15)	0.0666(12)	0.018(7)		
			0.06211(26)	0.130(6)	0.031(12)		
			0.09033(35)	0.186(7)	0.043(20)		
			0.1215(6)	0.252(16)	0.046(13)		

3.0	1.07	0.35	0.003325(11)	0.01079(10)	0.0006(5)
			0.03182(8)	0.1033(31)	0.0047(40)
			0.06244(14)	0.205(8)	0.008(9)
			0.09076(6)	0.302(17)	0.009(10)
			0.12192(48)	0.417(17)	0.008(11)
		0.514	0.003321(14)	0.01076(15)	0.0008(7)
			0.03178(7)	0.1034(22)	0.0069(32)
			0.06233(11)	0.203(8)	0.013(6)
			0.09067(15)	0.301(12)	0.017(6)
			0.12170(48)	0.416(19)	0.019(15)
		0.65	0.003315(12)	0.01073(12)	0.0011(6)
			0.03172(9)	0.1031(25)	0.0099(47)
			0.06216(13)	0.203(6)	0.020(6)
			0.09050(7)	0.302(13)	0.024(7)
			0.12150(18)	0.412(19)	0.027(5)
	2.1	0.35	0.003258(47)	0.01054(19)	0.0008(26)
			0.01548(15)	0.0504(13)	0.006(8)
			0.03111(20)	0.1018(25)	0.011(11)
			0.04702(27)	0.1509(32)	0.009(15)
			0.06231(24)	0.202(12)	0.010(13)
			0.09359(35)	0.314(19)	0.012(20)
			0.12418(26)	0.418(23)	0.013(33)
		0.514	0.00325(5)	0.01050(15)	0.0012(31)
			0.01543(15)	0.0505(14)	0.008(8)
			0.03102(23)	0.1016(27)	0.015(13)
			0.04690(28)	0.1509(40)	0.014(15)
			0.06216(24)	0.203(12)	0.018(14)
			0.09337(34)	0.314(19)	0.024(20)
			0.12387(29)	0.415(25)	0.029(33)
		0.65	0.003241(47)	0.01048(21)	0.0017(27)
			0.01541(18)	0.0503(16)	0.009(10)
			0.03094(25)	0.1009(29)	0.019(14)
			0.04680(37)	0.1505(47)	0.019(20)
			0.06201(24)	0.203(12)	0.025(13)
			0.09318(35)	0.314(19)	0.032(21)
			0.1237(6)	0.417(22)	0.038(37)
	3.98	0.35	0.003228(35)	0.010458(30)	0.0013(19)
			0.01549(7)	0.05052(48)	0.0047(41)
			0.03030(17)	0.0978(18)	0.010(10)
			0.04593(28)	0.1497(41)	0.014(17)
			0.05938(46)	0.196(12)	0.022(23)
			0.08934(20)	0.293(12)	0.013(22)
			0.1188(7)	0.400(14)	0.021(31)
		0.514	0.003210(44)	0.01039(16)	0.0022(25)
			0.01543(11)	0.0502(9)	0.008(7)
			0.03017(24)	0.0974(20)	0.017(14)
			0.04577(35)	0.149(6)	0.022(19)
			0.05910(49)	0.195(11)	0.033(27)
			0.08892(49)	0.292(13)	0.031(31)
			0.1184(6)	0.397(21)	0.040(31)

		0.65	0.00320(6)	0.01033(20)	0.0028(33)
			0.01537(6)	0.0500(7)	0.011(5)
			0.03006(26)	0.0971(21)	0.022(15)
			0.04562(22)	0.148(5)	0.029(13)
			0.0589(5)	0.194(11)	0.045(26)
			0.08862(37)	0.291(12)	0.044(24)
			0.1118(6)	0.397(21)	0.056(31)

Figures

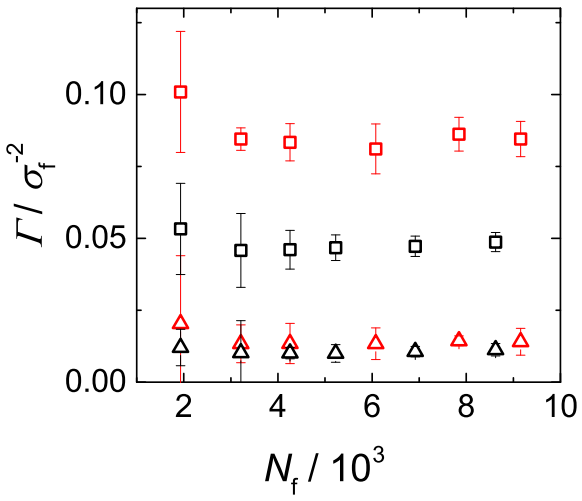

Figure 1: Surface excess Γ as a function of the number of fluid particles N_f for temperature T =0.7 ε_f/k (red) and T =0.8 ε_f/k (black), and reduced solid-fluid interaction energy $\zeta = 0.35$ ($\triangle$) and $\zeta = 0.65$ ($\square$). [This Figure is 1 column wide]

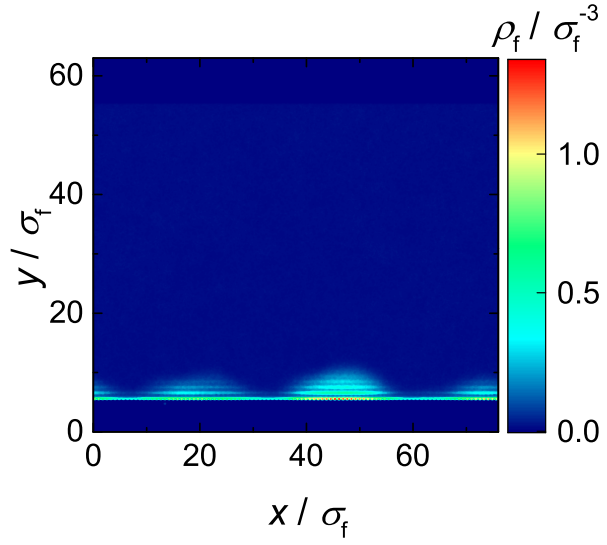

Figure 2: Density field $\rho_f(y, x)$ averaged in z-direction. [This Figure is 1 column wide]

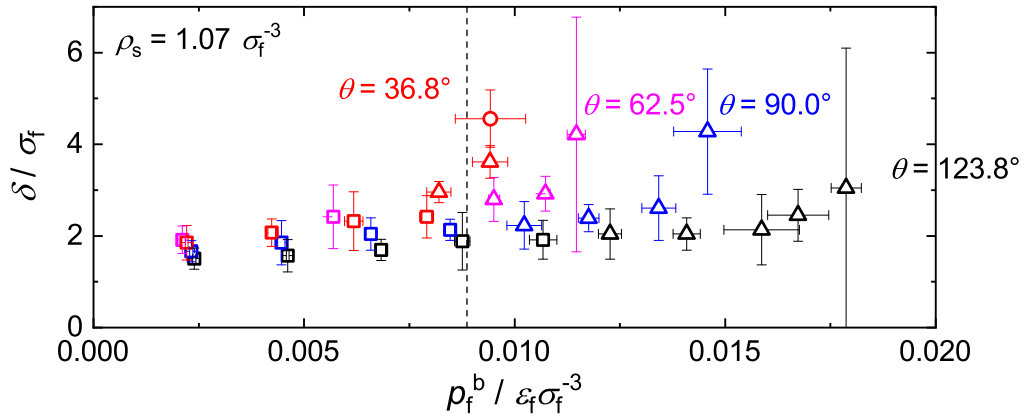

Figure 3: Adsorption layer thickness for $T/T_c = 0.7$ and $\rho_s = 1.07\ \sigma_f^{-3}$. The simulation data is shown as symbols, the uncertainty is indicated by error bars. The number of peaks in the adsorption layer is shown with different symbols: one peak (□), two peaks (△), and three peaks (◯). The saturation pressure is shown as a black dashed line. $W = 1.08$ (black), $W = 1.58$ (blue), $W = 2.00$ (violet), and $W = 2.31$ (red). [This Figure is 2 columns wide]

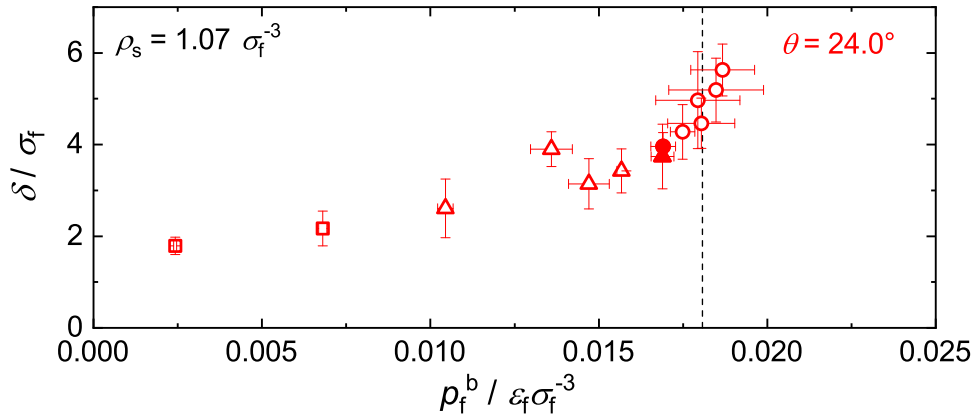

Figure 4: Adsorption layer thickness for $T/T_c = 0.77$ and $\rho_s = 1.07\ \sigma_f^{-3}$. The simulation data is shown as symbols, the uncertainty is indicated by error bars. The number of peaks in the adsorption layer is shown with different symbols: one peak (□), two peaks (△), and three peaks (◯). The saturation pressure is shown as a black dashed line. $W = 2.31$ (red). [This Figure is 2 columns wide]

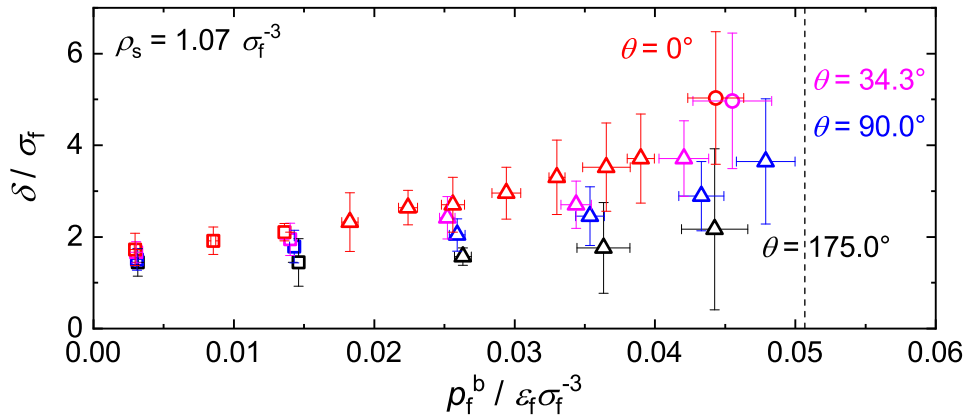

Figure 5: Adsorption layer thickness for $T/T_c = 0.9$ and $\rho_s = 1.07\ \sigma_f^{-3}$. The simulation data is shown as symbols, the uncertainty is indicated by error bars. The number of peaks in the adsorption layer is shown with different symbols: one peak (□), two peaks (△), and three peaks (◯). The saturation pressure is shown as a black dashed line. $W = 1.08$ (black), $W = 1.58$ (blue), $W = 2.00$ (violet), and $W = 2.31$ (red). [This Figure is 2 columns wide]